



MASTER THESIS 2013

SUBJECT AREA: Structural Dynamics	DATE: 06.06.2013	NO. OF PAGES: 85
--------------------------------------	---------------------	---------------------

TITLE:

**Wind Induced Dynamic Response of Concrete Box Girders During a
Balanced Cantilevered Construction Stage**

Vindindusert dynamisk respons for frittrembyggbroer i byggefasen

BY:

Martine Øien Helliesen



SUMMARY:

In this thesis a theoretical study of wind induced dynamic response of line-like structures has been performed, followed up by calculations of the dynamic response of Dolmsundet Bridge in its critical construction stage. Dolmsundet Bridge is constructed by the balanced cantilever method, which implies that until the cantilevered girders are connected to an adjacent cantilever or supports on shore all forces on the girder must be obtained by the pillar as moment and torsional stress. Thus is the construction particularly vulnerable against wind.

The theoretical study focuses on a frequency domain approach of the calculation of buffeting and vortex shedding induced dynamic response of line-like structures. Some statistical principles and a stochastic description of the turbulent wind must be presented before expressions of the loads and thereafter the response due to vortex shedding and buffeting wind can be derived. A section showing how the cross sectional forces can be divided into a resonant and a background part in order to reduce inaccuracy is also included.

A MATLAB program is composed to perform the calculations of the wind induced dynamic response of Dolmsundet Bridge in the construction stage. The response due to the first two modes is calculated, and time domain simulations of the displacements at the tip of the longest cantilever are created in order to find the maximum values. The calculations show that vortex shedding would be the most important phenomenon for the mode in the vertical direction.

Several assumptions and simplifications are made, possibly introducing inaccuracy. It is discussed possible sources of errors and to what extent selected parameters will affect the result. It was found that the structural damping had less influence on the calculated response. The vortex shedding parameters, and especially the nondimensional root mean square lift coefficient, could represent a source of error, and must be chosen with care. It was also discovered that galloping might be an issue due to negative lift derivatives. There should be performed investigations towards ensuring that the aerodynamic damping does not significantly reduce the total damping.

RESPONSIBLE TEACHER: Einar N. Strømmen

SUPERVISOR: Einar N. Strømmen

CARRIED OUT AT: Norwegian University of Science and Technology, Department of Structural Engineering

MASTEROPPGAVE 2013

Konstruksjonsteknikk

for

Martine Øien Helliesen

VINDINDUSERT DYNAMISK RESPONS FOR FRITT-FREMBYGG- BROER I BYGGEFASEN

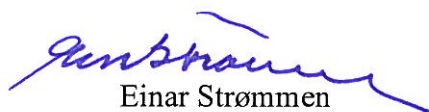
Wind-induced dynamic response of concrete box girders during a balanced cantilevered construction stage

En av de mest vanlige brotypene som bygges her i landet er de såkalte «frittfrembyggbroene». Dette er betongbroer med rektangulært kassetverrsnitt (med variabel høyde i spennretningen og utstikkende fortau), som har fått sin betegnelse fordi de bygges ved at brobjelken utkrages fra pilarene på hver side av brospennet til de kan forankres til landkarene og sammenknytning kan finne sted på midten. For den mest kritiske byggetilstanden vil altså brobjelke og pilar på hver side av krysningen danne en frittstående utkraget T som i en kort periode må kunne tåle å stå alene. For mange aktuelle spenn representerer denne byggetilstanden en kritisk fase med hensyn til påkjenninger på grunn av vind, bl.a. fordi det kan komme til å oppstå betydelige svingninger av brobjelken. Slike svingninger vil forekomme både i vindretningen og på tvers av vindretningen, og de vil derfor kunne medføre kritiske bøye- og torsjonspåkjenninger i pilaren. Det er i løpet av de siste årene gjort betydelig innsats for å kvantifisere de aerodynamiske effektene som oppstår for denne situasjonen. En av de oppgavene som gjenstår er å generalisere de dynamiske lastegenskapene, og å gjøre tilgjengelig data egnet til aktuelle beregningsrutiner. Hensikten med denne oppgaven er å foreta et litteraturstudium med sikte på å kartlegge de nødvendige lastparametrene som vil være nødvendig å kvantifisere for å kunne foreta en realistisk beregning av dynamisk respons, i vertikal- og horisontalretningen på tuppen av brobjelken. Oppgaven foreslås lagt opp etter følgende plan:

1. Studenten skal sette seg inn i virkning og byggemåte av frittfrembyggbruer.
2. Det foretas et litteraturstudium med sikte på å skaffe seg kjennskap til teoriene for beregning av vindindusert dynamisk last og lastvirkninger for turbulens og virvelavløsning, og eventuelt den dynamiske lastvirkningen som i litteraturen går under betegnelsen "galloping".
3. Det utarbeides et Matlab regnemaskinprogram som beregner de responsstørrelsene som er nødvendige for å kunne foreta en tilstrekkelig sikkerhetsvurdering av systemet.
4. I samarbeid med Dr. ing. Bjørn Isaksen i Vegdirektoratet skal det foretas en beregning på Sandsfjordbrua (eller et lignende system). I den grad tiden tillater det skal beregningene munne ut i anbefalinger for å kunne håndtere den uheldige effekten av de vindinduserte svingningene.

Studenten kan selv velge hvilke problemstillinger han ønsker å legge vekt på. Oppgaven skal gjennomføres i samarbeid med Siv.ing. Kristian Berntsen og Dr.ing. Bjørn Isaksen i Vegdirektoratet.

NTNU, 2013-01-03


Einar Strømmen

Summary

In this thesis a theoretical study of wind induced dynamic response of line-like structures has been performed, followed up by calculations of the dynamic response of Dolmsundet Bridge in its critical construction stage. Dolmsundet Bridge is constructed by the balanced cantilever method, which implies that until the cantilevered girders are connected to an adjacent cantilever or supports on shore all forces on the girder must be obtained by the pillar as moment and torsional stress. Thus is the construction particularly vulnerable against wind.

The theoretical study focuses on a frequency domain approach of the calculation of buffeting and vortex shedding induced dynamic response of line-like structures. Some statistical principles and a stochastic description of the turbulent wind must be presented before expressions of the loads and thereafter the response due to vortex shedding and buffeting wind can be derived. A section showing how the cross sectional forces can be divided into a resonant and a background part in order to reduce inaccuracy is also included.

A MATLAB program is composed to perform the calculations of the wind induced dynamic response of Dolmsundet Bridge in the construction stage. The response due to the first two modes is calculated, and time domain simulations of the displacements at the tip of the longest cantilever are created in order to find the maximum values. The calculations show that vortex shedding would be the most important phenomenon for the mode in the vertical direction.

Several assumptions and simplifications are made, possibly introducing inaccuracy. It is discussed possible sources of errors and to what extent selected parameters will affect the result. It was found that the structural damping had less influence on the calculated response. The vortex shedding parameters, and especially the nondimensional root mean square lift coefficient, could represent a source of error, and must be chosen with care. It was also discovered that galloping might be an issue due to negative lift derivatives. There should be performed investigations towards ensuring that the aerodynamic damping does not significantly reduce the total damping.

Norsk sammendrag

Denne masteroppgaven består av en litteraturstudie av vindindusert dynamisk respons av linjekonstruksjoner, etterfulgt av beregninger av dynamisk respons for Dolmsundbrua i sin kritiske byggefase. Dolmsundbroa bygges som en frittrembyggbro, hvor to utkragerer monteres symmetrisk ut fra en pilar. På tidspunktet rett før utkragerne blir koblet til en tilstøtende utkrager eller mot landkar vil alle kreftene på broa måtte tas opp som torsjon og moment i pilaren. I denne delen av byggefasen er broa derfor spesielt sårbar for vind.

Litteraturstudiet fokuserer på beregninger av turbulens-, og virvelavløsningsindusert dynamisk respons av linjekonstruksjoner i frekvensdomenet. Noen statistiske begreper og en stokastisk beskrivelse av vinden er presentert før fremgangsmåter for beregning av laster og respons fra turbulens og virvelavløsning er presentert. Det er også inkludert et kapittel hvor det er beskrevet hvordan beregninger av tverrsnittskrefter kan deles opp i en bakgrunnsdel og en resonant del for å fjerne unøyaktighet.

Et MATLAB regneprogram er laget for å utføre beregningene av den vindinduserte dynamiske responsen for Dolmsundbroa i byggefasen. Det er utført beregninger av responsen grunnet de to laveste svingemodene, den første i vindretningen og den andre i vertikalretningen. Det er benyttet tidssimuleringer av responsen ytterst på den lengste utkrageren for å finne maksimalverdier. Beregningene viser at virvelavløsning vil være det viktigste fenomenet for moden med hovedkomponent i vertikalretningen.

Det er gjort flere antagelser og forenklinger som kan introdusere feil i resultatet. Det er diskutert mulige feilkilder og sett på hvor sensitivt resultatet er for endringer i enkelte av de usikre parametrene. Det ble funnet resultater som tydet på at egendempingen av konstruksjonen hadde liten betydning for den totale responsen. Virvelavløsningsparametrene, og spesielt den dimensjonsløse rotmiddelkvadrerte løftkoeffisienten, kan representere en feilkilde og må velges med omhu da de vil ha stor innvirkning på den beregnede responsen. Det ble også oppdaget at fenomenet "galloping" kan være et problem på grunn av negative deriverte av løftkoeffisienter. Det bør gjøres undersøkelser for å forsikre at den aerodynamiske dempingen ikke nevneverdig reduserer den totale dempingen.

Preface

This master thesis marks the end of my five years Master's Degree Programme in Civil and Environmental Engineering at the Norwegian University of Science and Technology. The thesis is written for the Department of Structural Engineering and corresponds to 30 credits.

The object of the thesis is to acquire knowledge about wind induced dynamic response of line-like structures, by performing a theoretical study followed up by calculations of a concrete example. This requires understanding of both mechanics, numerics, computer programming and statistics, such that I got to use and develop large parts of the knowledge I have acquired during these five years of studies.

I would like to thank my supervisor Einar N. Strømmen for his guidance and inspiration. His book *Theory of Bridge Aerodynamics* [1] has been the most important source of information during this work.

I would also like to thank the Norwegian Public Roads Administration for providing me important input for the calculations.

Trondheim, 06.06.2013

Martine Øien Helliesen

Contents

1	Theory	1
1.1	Introduction	1
1.2	Statistical Concepts of Stochastic Processes	1
1.2.1	Maximum Values	2
1.2.2	Variance and Spectral Density	3
1.2.3	Covariance and Cross Spectral Density	6
1.2.4	Coherence	6
1.3	Stochastic Description of Turbulent Wind	7
1.3.1	Mean Wind Velocity	9
1.3.2	Kaimal Spectral Density	9
1.3.3	Normalized Co-Spectrum	11
1.4	Wind Induced Loads	11
1.4.1	Buffeting Theory	12
1.4.2	Vortex Shedding	14
1.5	Response Calculations	16
1.5.1	Dynamic Equilibrium and Frequency Response Function	16
1.5.2	Response Spectrum	18
1.5.3	Buffeting Response	18
1.5.4	Vortex Shedding Response	21
1.6	Determination of Cross Sectional Forces	24
1.6.1	Background Part	25
1.6.2	Resonant Part	28
1.7	Time Domain Simulations	30
2	Calculations	31
2.1	Introduction	31
2.2	Balanced Cantilever Bridges	31
2.3	General Assumptions and Simplifications	32
2.4	Properties of Dolmsundet Bridge	33
2.5	Buffeting Response Calculations	35
2.5.1	Properties of the Turbulent Wind	35
2.5.2	Load Coefficients	37
2.5.3	Frequency Response	38
2.5.4	Buffeting Load Spectrum	39
2.5.5	Buffeting Response	40
2.6	Vortex Shedding Calculations	42
2.6.1	Simplified Model	43
2.6.2	Properties of the Vortex Shedding Induced Wind Loads	44
2.6.3	Aerodynamic Damping	44
2.6.4	Vortex Shedding Load Spectrum	45
2.6.5	Vortex Shedding Response	46
2.7	Maximum Displacements	48

3	Sources of Errors	50
3.1	Wind on Pillar	50
3.2	Elevation Height	50
3.3	Load Coefficients	51
3.4	Motion Induced Effects	52
3.5	Buffeting Co-Spectrum	53
3.6	Vortex Shedding Parameters	53
3.7	Structural Damping	55
3.8	Numerical Integration	55
4	Conclusion	57
5	Suggestions for Further Research	59
A	Definition of Elements	a
B	Inputfile	b
C	MATLAB Scripts	c

1 Theory

1.1 Introduction

When wind meets an obstacle forces will occur. These forces may in broad terms be ascribed to different phenomenons: the wind will fluctuate, causing buffeting loads; vortex shedding may be created due to irregularities on the obstacle's surface; and also the obstacle may oscillate and interact with the wind fluctuations and create so-called motion induced forces. From a structural engineering point of view it is important that the displacements are minor, and that the capacity through the lifetime of the construction is large enough to resist the wind induced loads.

The following sections will describe the theory behind buffeting- and vortex shedding induced dynamic response of a line-like structure. While the largest dynamic response from buffeting wind will occur at the maximum wind velocity, vortex shedding induced dynamic response will be largest for lower wind velocities. It is therefore common to treat the two phenomena separately even though both to some extent are present and will interact when a line-like structure is exposed to wind.

The wind induced forces on a structure are described on the background of Bernoulli's principle of energy conservation in a fluid. The theory will end in a frequency domain method of calculating the displacements and the cross sectional forces of a line-like structure exposed to a turbulent wind field. It is presupposed an undisturbed wind field and linear elastic structural behavior.

The wind is usually conservatively assumed perpendicular to the line-like structure, but the magnitude of the wind velocity is more or less random in time and space. A time series describing the mean wind velocity will not be similar to another even though the conditions are exactly the same, but it will follow a certain pattern. This pattern is described by statistical properties, and is denominated a stochastic process. In order to understand the theory behind wind induced dynamic response some statistical concepts must first be presented.

1.2 Statistical Concepts of Stochastic Processes

As described in the introduction, wind is a stochastic process. A stochastic process has the characteristic feature that its outcome never can be predicted exactly, it can only be predicted with a certain probability. When performing a dynamic analysis it is important that the time window of the stochastic process is short enough to assume stationary and homogeneous statistical properties. Usually the wind is measured over periods of 10 minutes.

The velocity of the wind is the interesting variable regarding wind loads. The wind velocity may be described as a sum of a mean part and a fluctuating part. It is a normal

assumption that the fluctuating part of the wind velocity has a Gaussian probability distribution around the mean value, see figure 1.1.

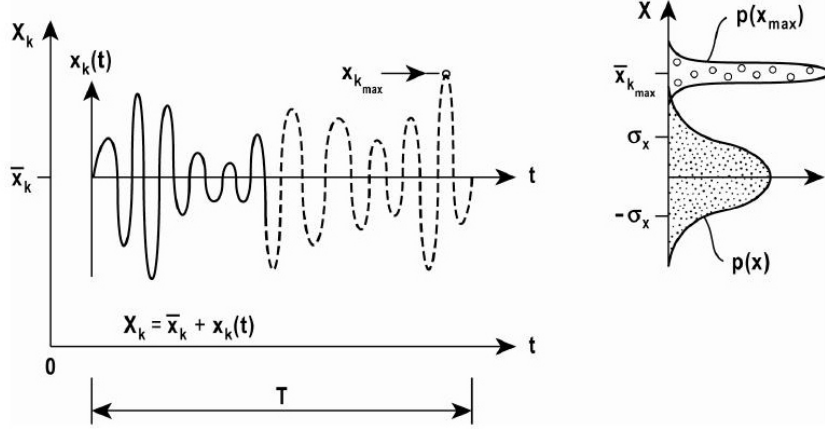


Figure 1.1: Graphical representation of a stochastic process during a short time window [1, page 4]

Further in this report it is assumed that load effects, response and cross sectional forces are linearly dependent on the wind velocity and thus will be stochastic processes with a Gaussian probability distribution.

Below a couple of statistical principles of stochastic processes will be presented.

1.2.1 Maximum Values

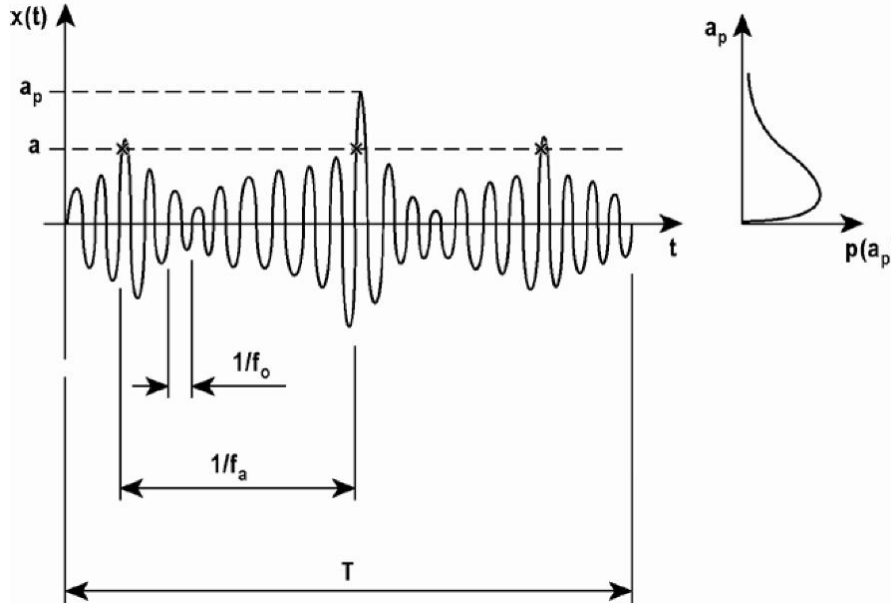
The peak factor is introduced to give an expression of the maximum value of a stochastic process that statistically will occur once during a certain time window. Figure 1.2 shows a realization of a stochastic process with a mean value of zero during a time window T .

It may be observed that the number of peaks during the time window is $f_x(0) \cdot T$, where $f_x(0)$ is the average zero up-crossing frequency. For narrow banded processes $f_x(a_p) \cdot T$ will be the expected number of peaks larger than a_p and must obtain the value 1 in order to find the maximum value, $x_{max} = a_p$, that will occur only once within the time frame. It may be shown that the mean x_{max} for several realizations of the stochastic process with zero mean value is given by [1, page 31]

$$\bar{x}_{max} = k_p \cdot \sigma_x = \left\{ \sqrt{2 \cdot \ln [f_x(0) \cdot T]} + \frac{\gamma}{\sqrt{2 \cdot \ln [f_x(0) \cdot T]}} \right\} \cdot \sigma_x \quad (1.1)$$

where $\gamma \approx 0.5772$ is the Euler constant.

For a stochastic process with mean value \bar{x} this will render a maximum value of

Figure 1.2: Stochastic process with maximum value a_p [1, page 28]

$$X_{max} = \bar{x} + k_p \cdot \sigma_x \quad (1.2)$$

where the peak factor, k_p is

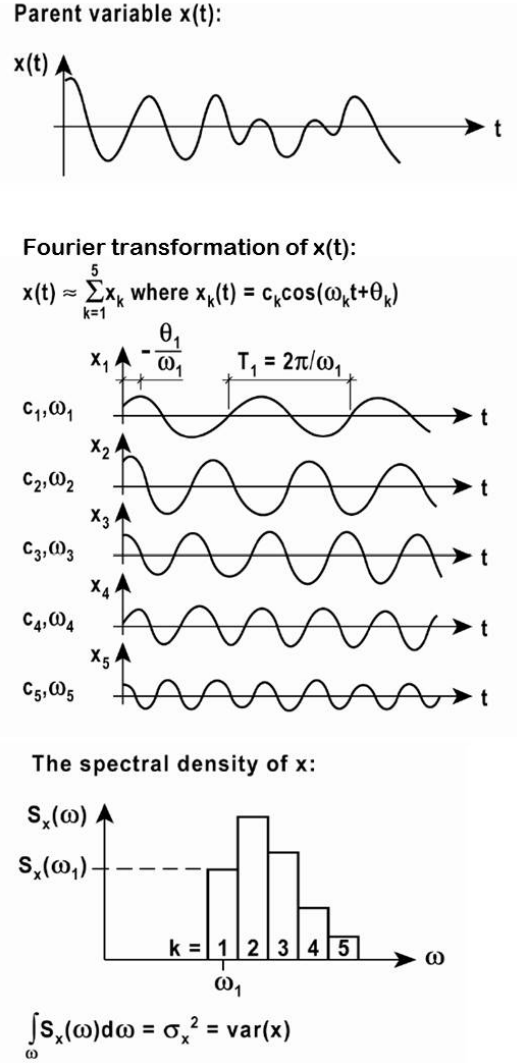
$$k_p = \left\{ \sqrt{2 \cdot \ln [f_x(0) \cdot T]} + \frac{\gamma}{\sqrt{2 \cdot \ln [f_x(0) \cdot T]}} \right\} \quad (1.3)$$

When the stochastic process is ultra narrow banded it can be described by the harmonic expression $X(t) = c_x \cdot \cos(\omega_x t)$, which will render a standard deviation $\sigma_x = c_x / \sqrt{2}$, and thus a peak factor $k_p = \sqrt{2}$. Equation (1.3) is therefore only valid for fairly broad banded processes.

The peak factor is often found directly from time domain simulations. If a reasonable number of simulations are performed, the average max value divided on the standard deviation will give a good approximation of the peak factor.

1.2.2 Variance and Spectral Density

The variance of a stochastic process can be found by using a frequency domain approach and the concept of auto spectral density. Auto spectral density describes the weighting of the amplitudes of the different frequencies a stochastic process consists of, see figure 1.3.

Figure 1.3: The auto spectral density of a stochastic process $x(t)$ [1, page 35]

The auto spectral density of a harmonic function $X_k(t) = c_k \cos(\omega_k t + \theta_k)$ with frequency ω_k and mean value equal to zero is given by

$$S_x(\omega_k) = \frac{E[X_k^2]}{\Delta\omega} = \frac{\sigma_{X_k}^2}{\Delta\omega} \quad (1.4)$$

The variance of the harmonic function is from a time domain approach defined by

$$\sigma_{X_k}^2 = \lim_{T \rightarrow \infty} \int_0^T [c_k \cos(\omega_k t + \phi_k)]^2 dt \quad (1.5)$$

By replacing T with $n \cdot T_k$, where $T_k = 2\pi/\omega_k$ and $n \rightarrow \infty$, the auto spectral density of the harmonic function is obtained

$$\begin{aligned} S_x(\omega_k) &= \lim_{T \rightarrow \infty} \frac{1}{\Delta\omega} \cdot \frac{1}{T} \int_0^T [c_k \cos(\omega_k t + \phi_k)]^2 dt \\ &= \lim_{n \rightarrow \infty} \frac{1}{\Delta\omega} \cdot \frac{1}{n \cdot T_k} \cdot n \int_0^{T_k} \left[c_k \cos\left(\frac{2\pi}{T_k} \cdot t + \phi_k\right) \right]^2 dt = \frac{c_k^2}{2\Delta\omega} \end{aligned} \quad (1.6)$$

The variance of the stochastic process $x(t)$ may be found by Fourier transformation, where $x(t)$ is approximated a sum of harmonic functions $X_k(\omega_k, t)$, and the auto spectral density of each of these are summarized. When performing this on a significant number of frequencies, i.e. $N \rightarrow \infty$ and $\Delta\omega \rightarrow d\omega$, the variance of $x(t)$ is obtained

$$\sigma_x^2 = \sum_{k=0}^{N \rightarrow \infty} S_X(\omega_k) \Delta\omega \approx \int_0^\infty S_x(\omega) d\omega \quad (1.7)$$

Auto spectral density may also be expressed in a complex format. The stochastic process $x(t)$ is then Fourier transformed into a sum of complex functions

$$x(t) = \sum_{-\infty}^{\infty} X_k(\omega_k, t) = \sum_{-\infty}^{\infty} d_k(\omega_k) \cdot e^{i\omega_k t} \quad (1.8)$$

For stationary processes with time length long enough to assume that the position of the time axis for integration is irrelevant, the Fourier constant of $X(\omega_k, t)$ may be introduced

$$a_k(\omega_k) = \int_0^T x_k(t) \cdot e^{-i\omega_k t} dt = T \cdot d_k \quad (1.9)$$

The auto spectral density of $\pm\omega_k$ is then

$$S_x(\pm\omega_k) = \frac{E[X_k^* \cdot X_k]}{\Delta\omega} = \frac{d_k^* \cdot d_k}{\Delta\omega} = \frac{(a_k^*/T) \cdot (a_k/T)}{2\pi/T} = \frac{1}{2\pi T} \cdot a_k^* a_k \quad (1.10)$$

The auto spectral density of any ω can be found by inserting the limit values T and $N \rightarrow \infty$. The single sided version is obtained by multiplying the result by 2

$$S_x(\omega) = \lim_{T \rightarrow \infty} \frac{1}{\pi T} \cdot a^*(\omega) \cdot a(\omega) \quad (1.11)$$

1.2.3 Covariance and Cross Spectral Density

The cross spectral density is the frequency domain counterpart of covariance as the auto spectral density is of variance. It can be derived as above, starting with a Fourier transformation of the two stochastic processes with zero mean value, $x(t) = \sum_{-\infty}^{\infty} X_k(\omega_k, t)$ and $y(t) = \sum_{-\infty}^{\infty} Y_k(\omega_k, t)$. The cross spectral density of the two functions for the frequency ω_k is [1, page 38]

$$S_{xy}(\pm\omega_k) = \frac{E[X_k^* \cdot Y_k]}{\Delta\omega} = \frac{1}{2\pi T} \cdot a_{X_k}^* a_{Y_k} \quad (1.12)$$

The covariance of the two stochastic processes is by definition

$$Cov_{xy} = E[x(t) \cdot y(t)] = E\left[\left(\sum_{-\infty}^{\infty} X_i(\omega_i, t)\right) \cdot \left(\sum_{-\infty}^{\infty} Y_j(\omega_j, t)\right)\right] \quad (1.13)$$

For any $\omega_i \neq \omega_j$ the value of $E[X_i(\omega_i, t) \cdot Y_j(\omega_j, t)]$ will be zero when the two functions are independent. Thus is the covariance

$$Cov_{xy} = \sum_{-\infty}^{\infty} (E[X_k \cdot Y_k]) = \sum_{-\infty}^{\infty} S_{xy}(\pm\omega_k) \cdot \Delta\omega \approx \int_0^{\infty} S_{xy}(\omega) d\omega \quad (1.14)$$

The covariance may also be defined from different realizations of the same process $x(t)$ at a distance Δs and a time gap τ from each other

$$Cov_{xx}(\Delta s, \tau) = E[x(s, t) \cdot x(s + \Delta s, t + \tau)] = \lim_{T \rightarrow \infty} \frac{1}{T} \int_0^T x(s, t) \cdot x(s + \Delta s, t + \tau) dt \quad (1.15)$$

A normalized version of this is the cross covariance coefficient defined by

$$\rho_{xx}(\Delta s, \tau) = \frac{Cov_{xx}(\Delta s, \tau)}{\sigma_x^2} \quad (1.16)$$

1.2.4 Coherence

Coherence describes how harmonized the waves from different processes are. The coherence between the stochastic processes $x(t)$ and $y(t)$ is defined by [1, page 42]

$$Coh_{xy}(\omega) = \frac{|S_{xy}(\omega)|^2}{S_x(\omega) \cdot S_y(\omega)} \quad (1.17)$$

where $S_{xy}(\omega)$ is the cross spectral density as described in 1.2.3.

It is common to define a normalized co-spectrum, which is the square root of the coherence function with imaginary parts cancelled out

$$\hat{C}_{oxy}(\omega) = \frac{\text{Re}[S_{xy}(\omega)]}{\sqrt{S_x(\omega) \cdot S_y(\omega)}} \quad (1.18)$$

It is seen that if $x(t)$ and $y(t)$ describes the same process the real part of the cross spectrum will be given by

$$\text{Re}[S_{xx}(\omega)] = S_x(\omega) \cdot \hat{C}_{oxx}(\omega) \quad (1.19)$$

1.3 Stochastic Description of Turbulent Wind

The instantaneous wind velocity vector may be described by the sum of two functions of the flow coordinates (x_f, y_f, z_f) where x_f is defined in the direction of the flow, y_f perpendicular to the flow in the horizontal direction and z_f perpendicular to the flow in the vertical direction. The first function, V , represents the mean wind velocity in the along wind direction, and the second function represents the turbulent part in the directions along the wind, u , and perpendicular to the wind, v and w . The turbulent parts are described by fluctuating functions dependent on the time and position and with a mean value equal to zero.

$$U(x_f, y_f, z_f, t) = V(x_f, y_f, z_f) + u(x_f, y_f, z_f, t), v(x_f, y_f, z_f, t) \text{ and } w(x_f, y_f, z_f, t) \quad (1.20)$$

When looking at bridges the main flow direction is assumed perpendicular to the span, and the span direction is usually defined as the x -axis, i.e. the x -axis coincides with flow direction y_f and the y -axis with flow direction x_f , as illustrated in figure 1.4. The height above ground, z_f , can usually be approximated a constant value. The fluctuating part in the span direction, w , will be of no interest. The expression of the wind velocity vector in the position x along the bridge span may then be simplified to

$$U(x, t) = V + u(x, t) \text{ and } w(x, t) \quad (1.21)$$

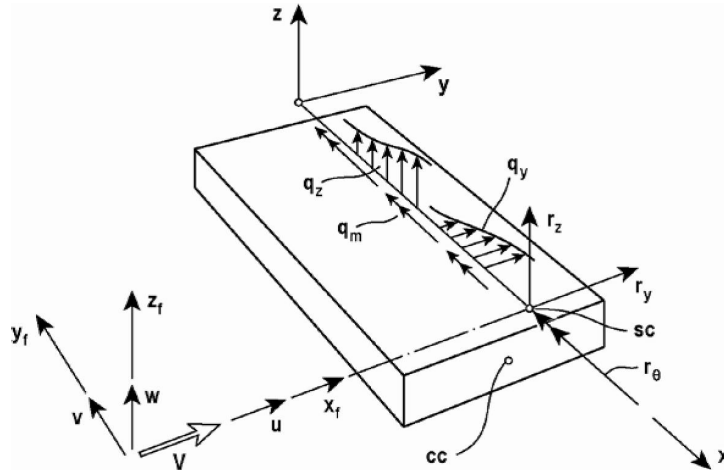


Figure 1.4: Definition of flow and structural axes [1, page 6]

This function is assumed to fulfill the criteria of a Gaussian probability distribution with mean value V and variances σ_u^2 and σ_w^2 in respectively y - and z -direction. Figure 1.5 shows the wind velocity in the along wind direction over a period T , usually 10 minutes, at a specific point along the bridge span.

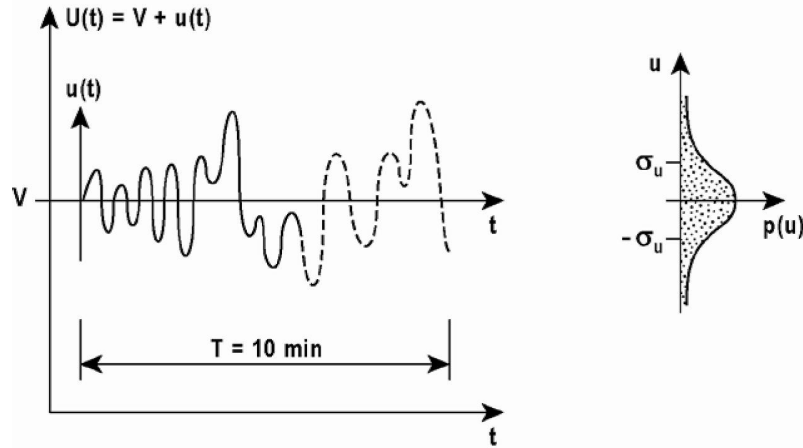


Figure 1.5: Graphical representation with accompanying probability distribution of the wind velocity in the along wind direction [1, page 59]

When calculating the dynamic forces on a wind exposed structure there are three levels of statistical properties that are of interest. It is the long term variation of wind expressed by the mean wind velocity, the short term single point variation of the turbulent parts, expressed by the auto spectral density, and the short term spatial distribution of the turbulent parts, expressed by the coherence. These will be discussed below.

1.3.1 Mean Wind Velocity

Experiments have shown that a good approximation of the 10 minutes mean wind velocity in the position z_f above the ground level may be given as [1, page 54]

$$\begin{aligned} \frac{V_{10}(z_f)}{V_r} &= k_T \ln \left(\frac{z_f}{z_0} \right) \quad \text{for } z_f > z_{min} \\ \frac{V_{10}(z_f)}{V_r} &= k_T \ln \left(\frac{z_{min}}{z_0} \right) \quad \text{for } z_f < z_{min} \end{aligned} \quad (1.22)$$

The value z_{min} is introduced because the formula will not be valid close to the ground due to turbulence effects. k_T and z_0 are parameters depending on the terrain. V_r is the reference wind, measured in a chosen reference height, usually 10 meters above ground level, and averaged through 10 minutes periods. When using the mean wind velocity in structural design one should collect data for several years. The data is usually fitted into a density distribution, for instance Weibull, Rayleigh or Fischer-Tippet [1, page 55], which is used to find the maximum 10 minutes mean wind value for a chosen return period, often 50 years.

1.3.2 Kaimal Spectral Density

The auto spectral density is used in order to describe the short term single point variation of the fluctuating parts of the wind. These fluctuating parts are assumed to have a zero mean Gaussian probability distribution with variance σ_n^2 , $n = u, v, w$. The variance may be found from the definition of turbulence intensity

$$I_n(z_f) = \frac{\sigma_n(z_f)}{V(z_f)} \quad \text{where } n = u, v, w \quad (1.23)$$

It may be shown that a good approximation of the intensity in the u-direction, i.e. in the along wind direction, is given by [1, page 59]

$$I_u(z_f) = \begin{cases} 1/\ln(z_f/z_0) & \text{for } z_f > z_{min} \\ 1/\ln(z_{min}/z_0) & \text{for } z_f < z_{min} \end{cases} \quad (1.24)$$

and that I_v and I_w in homogeneous terrain up to a height of 200 m above ground level is approximately

$$\begin{bmatrix} I_v \\ I_w \end{bmatrix} = \begin{bmatrix} 3/4 \\ 1/2 \end{bmatrix} \cdot I_u \quad (1.25)$$

Kaimal et. al. have proven that all turbulent wind have relatively similar spectral density distribution, depending on a couple of parameters, and have suggested the following expression of nondimensional auto spectral density [1, page 62]

$$\frac{f \cdot S_n(f)}{\sigma_n^2} = \frac{A_n \cdot \hat{f}_n}{\left(1 + 1.5 \cdot A_n \cdot \hat{f}_n\right)^{5/3}} \quad \text{where } n = u, v, w \quad (1.26)$$

Experiments have shown that for the parameter A_n the following values are applicable: $A_u = 6.8$ and $A_v = A_w = 9.4$. The normalized frequency is given by: $\hat{f}_n = f \cdot {}^{x_f}L_n/V$, where ${}^{x_f}L_n$ is the average length scale of the relevant turbulence component $n = u, v, w$ in the along wind direction. ${}^{x_f}L_n$ may be found from the average duration of a wind gust, T_n ,

$${}^{x_f}L_n = V \cdot T_n = V \cdot \int_0^\infty \rho_{nn}(\tau) d\tau \quad \text{where } n = u, v, w \quad (1.27)$$

where $\rho_{nn}(\tau)$ is the auto covariance coefficient defined in equation (1.16). For a turbulent wind field under homogeneous conditions the following expression is usually adopted [1, page 61]

$$\rho_{nn}(\Delta s = 0, \tau) = \exp(-\tau/T_n) \quad (1.28)$$

The auto covariance coefficient regarding variation in space, and not in time, is usually also approximated an exponential function [1, page 66]

$$\rho_{nn}(\Delta s, \tau = 0) = \exp(-\Delta s/{}^sL_n) \quad (1.29)$$

where $s = x_f, y_f, z_f$.

It has been shown that the following values of sL_n under homogeneous conditions and not unduly close to the ground are appropriate [1, page 66]

$$\begin{bmatrix} {}^{y_f}L_u \\ {}^{z_f}L_u \\ {}^{x_f}L_v \\ {}^{y_f}L_v \\ {}^{z_f}L_v \\ {}^{x_f}L_w \\ {}^{y_f}L_w \\ {}^{z_f}L_w \end{bmatrix} \approx \begin{bmatrix} 1/3 \\ 1/4 \\ 1/4 \\ 1/4 \\ 1/12 \\ 1/12 \\ 1/16 \\ 1/16 \end{bmatrix} \cdot {}^{x_f}L_u \quad (1.30)$$

where ${}^{x_f}L_u$ is

$$\begin{cases} x_f L_u(z_f) \approx x_f L_u(z_{f0}) \cdot \left(\frac{z_f}{z_{f0}}\right)^{0.3} \\ z_f > z_{f0} = 10 \text{ m} \\ x_f L_u(z_{f0}) = 100 \text{ m} \end{cases} \quad (1.31)$$

As the frequency usually is expressed in rad/s it is useful to write the expression of the nondimensional auto spectral density of the turbulent wind as a function of ω

$$\frac{\omega \cdot S_n(\omega)}{\sigma_n^2} = \frac{A_{n\omega} \cdot \omega \cdot x_f L_n}{V \left(1 + 1.5 \cdot A_{n\omega} \cdot \frac{\omega \cdot x_f L_n}{V}\right)^{5/3}} \quad (1.32)$$

where $A_{n\omega} = A_n/2\pi$ and $n = u, v, w$.

There are alternative spectral density distributions that might be employed, but it is chosen to use equation (1.32) further in this report.

1.3.3 Normalized Co-Spectrum

The normalized co-spectrum of a stochastic process $x(t)$ is described in section 1.2.4. Experiments have shown that a good approximation of the normalized co-spectrum of turbulent wind on a bridge span under homogeneous conditions is [1, page 67]

$$\hat{C}_{o_{nn}}(\Delta y_f, \omega) = \exp\left(-c_{ny_f} \cdot \frac{\omega \cdot \Delta y_f}{2\pi \cdot V(z_f)}\right) \quad (1.33)$$

where Δy_f is the separation length between the considered points along the bridge span, $V(z_f)$ is the mean wind velocity and the parameter c_{ny_f} is given by

$$\begin{aligned} c_{wy_f} &\approx 9 \\ c_{vy_f} &\approx c_{wy_f} \approx 6 \end{aligned} \quad (1.34)$$

1.4 Wind Induced Loads

As described in the introduction it is usually distinguished between calculations of response from buffeting, vortex shedding and motion induced loads because the three phenomena will dominate at different mean wind velocities. The response from motion induced loads is predominant for very large mean wind velocities, buffeting response is predominant for medium to large mean wind velocities, while large response from vortex shedding usually occur for lower mean wind velocities. In this section the theory behind

buffeting and vortex shedding induced loads will be presented, i.e. it is assumed that the wind velocity is below the instability limit. Buffeting wind gives response in both y -, z - and θ -direction, while vortex shedding response in y -direction is usually neglected.

1.4.1 Buffeting Theory

The buffeting theory is an established and widely accepted theory used to calculate loads on line-like structures exposed to a turbulent wind field. The theory is based on Bernoulli's equation in fluid dynamics [1, page 1-2]. The instantaneous forces that occur from wind exposure can be divided into three parts; drag in the in the along wind direction, lift in the direction perpendicular to the wind and moment trying to rotate the cross section. For a rectangular cross section with width B and height D , the three parts are given as

$$q_D(x, t) = \rho V_{rel}^2 D C_D(\alpha), \quad (1.35)$$

$$q_L(x, t) = \rho V_{rel}^2 B C_L(\alpha) \quad (1.36)$$

$$q_M(x, t) = \rho V_{rel}^2 B^2 C_M(\alpha) \quad (1.37)$$

where $C_D(\alpha)$, $C_L(\alpha)$ and $C_M(\alpha)$ are coefficients depending on the relative angle of flow incidence, α , as shown in figure 1.6.

The three load contributions may be transformed into loads in the directions of the structural axis by using the angle $\beta = \arctan\left(\frac{\omega - \dot{r}_z}{V + u - \dot{r}_y}\right)$

$$\mathbf{q}_{\text{tot}}(\mathbf{x}, \mathbf{t}) = \begin{bmatrix} q_y \\ q_z \\ q_\theta \end{bmatrix}_{\text{tot}} = \begin{bmatrix} \cos\beta & -\sin\beta & 0 \\ \sin\beta & \cos\beta & 0 \\ 0 & 0 & 1 \end{bmatrix} \begin{bmatrix} q_D \\ q_L \\ q_M \end{bmatrix} \quad (1.38)$$

Under normal circumstances the angle β will be small, and u and \dot{r}_y will be small compared to V . Accordingly will $\cos(\beta) \approx 1$ and $\sin(\beta) = \beta \approx (w - \dot{r}_z)/V$. Because u , w , \dot{r}_y and \dot{r}_z are small compared to V the product between them may be neglected and the relative wind velocity can be expressed by

$$V_{rel}^2 = (V + u - \dot{r}_y)^2 + (w - \dot{r}_z)^2 \approx V^2 + 2Vu - 2V\dot{r}_y \quad (1.39)$$

The angle α may be divided into a mean value and a fluctuating part, $\alpha = \bar{\alpha} + \alpha_f$, and the load coefficients may be written into the following linear approximation

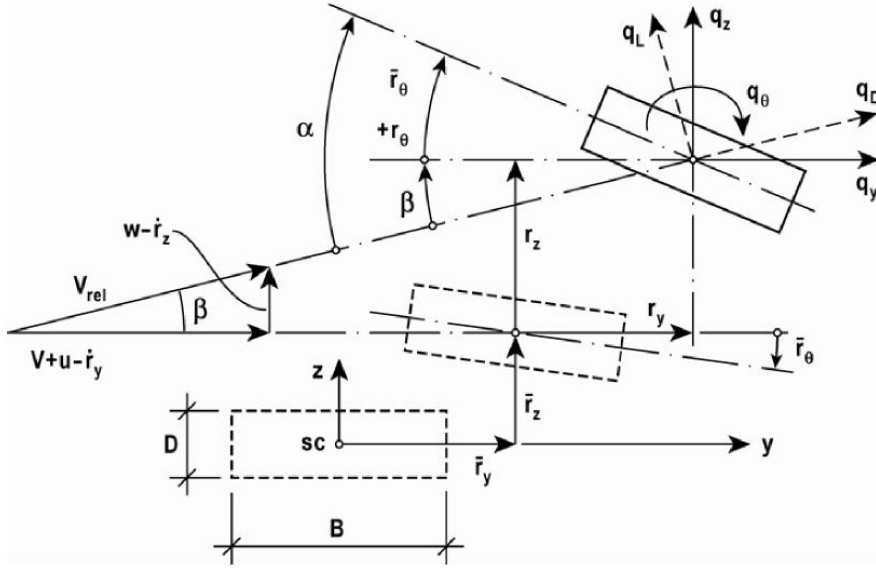


Figure 1.6: Instantaneous wind flow and displacements of a rectangular cross section [1, page 92]

$$\begin{bmatrix} C_D(\alpha) \\ C_L(\alpha) \\ C_M(\alpha) \end{bmatrix} = \begin{bmatrix} \bar{C}_D \\ \bar{C}_L \\ \bar{C}_M \end{bmatrix} + \alpha_f \cdot \begin{bmatrix} C'_D \\ C'_L \\ C'_M \end{bmatrix} \quad (1.40)$$

The expression of the total load \mathbf{q}_{tot} will be

$$\begin{bmatrix} q_y \\ q_z \\ q_\theta \end{bmatrix}_{tot} = \rho V \left(\frac{V}{2} + u - \dot{r}_y \right) \left(\begin{bmatrix} D\bar{C}_D \\ B\bar{C}_L \\ B^2\bar{C}_M \end{bmatrix} + \left(r_\theta + \frac{w}{V} - \frac{\dot{r}_z}{V} \right) \begin{bmatrix} DC'_D \\ BC'_L \\ B^2C'_M \end{bmatrix} + \frac{w - \dot{r}_z}{V} \begin{bmatrix} -B\bar{C}_L \\ D\bar{C}_D \\ 0 \end{bmatrix} \right) \quad (1.41)$$

which by neglecting the products of small terms may be written into

$$\mathbf{q}_{tot}(x, t) = \bar{\mathbf{q}} + \mathbf{B}_q \cdot \mathbf{v} + \mathbf{C}_{ae} \cdot \dot{\mathbf{r}} + \mathbf{K}_{ae} \cdot \mathbf{r} \quad (1.42)$$

where

$$\mathbf{v}(x, t) = \begin{bmatrix} u & w \end{bmatrix}^T \quad (1.43)$$

$$\mathbf{r}(x, t) = \begin{bmatrix} r_y & r_z & r_\theta \end{bmatrix}^T \quad (1.44)$$

$$\bar{\mathbf{q}}(x) = \begin{bmatrix} \bar{q}_y \\ \bar{q}_z \\ \bar{q}_\theta \end{bmatrix} = \frac{\rho V^2 B}{2} \begin{bmatrix} (D/B) \bar{C}_D \\ \bar{C}_L \\ B \bar{C}_M \end{bmatrix} \quad (1.45)$$

$$\mathbf{B}_q(x) = \frac{\rho V B}{2} \begin{bmatrix} 2(D/B) \bar{C}_D & \begin{pmatrix} (D/B) C'_D - \bar{C}_L \end{pmatrix} \\ 2\bar{C}_L & \begin{pmatrix} C'_L + (D/B) \bar{C}_D \end{pmatrix} \\ 2B\bar{C}_M & BC'_M \end{bmatrix} \quad (1.46)$$

$$\mathbf{C}_{ae}(x) = -\frac{\rho V B}{2} \begin{bmatrix} 2(D/B) \bar{C}_D & \begin{pmatrix} (D/B) C'_D - \bar{C}_L \end{pmatrix} & 0 \\ 2\bar{C}_L & \begin{pmatrix} C'_L + (D/B) \bar{C}_D \end{pmatrix} & 0 \\ 2B\bar{C}_M & BC'_M & 0 \end{bmatrix} \quad (1.47)$$

$$\mathbf{K}_{ae}(x) = \frac{\rho V^2 B}{2} \begin{bmatrix} 0 & 0 & (D/B) C'_D \\ 0 & 0 & C'_L \\ 0 & 0 & BC'_M \end{bmatrix} \quad (1.48)$$

Here does $\bar{\mathbf{q}}$ represent the static load, $\mathbf{B}_q \cdot \mathbf{v}$ the dynamic load and $\mathbf{C}_{ae} \cdot \dot{\mathbf{r}}$ and $\mathbf{K}_{ae} \cdot \mathbf{r}$ the motion induced loads. The two last terms appear because the structure is fluctuating, which alter the relative wind on the structure. Seeing that the last two terms depend on the displacements they must be transferred to the left side of the equilibrium equation, this is further discussed in section 1.5.1.

1.4.2 Vortex Shedding

Vortex shedding is a phenomenon that occurs when the wind flow is separated in the meeting of a cross section causing vortices on alternate sides. The horizontal displacement of bridge beams from vortex shedding is usually neglected, while vertical displacement and rotation may have great impact on a structure's total wind response. Investigations on stiff models have proven that the load from vortex shedding is narrow banded around a so-called vortex shedding frequency which is proportional to the wind velocity, V , divided by the cross sectional height, D ,

$$f_s = St \cdot \frac{V}{D} \quad (1.49)$$

where St is the so-called Strouhal number, depending on the type of cross section, and $f_s = \omega_s/2\pi$.

For flexible structures the largest response will naturally occur when the eigenfrequencies coincide with the vortex shedding frequencies. Significant motion induced forces may then occur and consequently will the damping properties of the structure be important. Vortex vibrations have the characteristic of being self-limiting, because when the displacements turn larger the motion induced load part will work against the wind load and thereby limit the displacements.

Vickery & Basu have suggested a mathematical expression of the single point load spectrum of vortex shedding exposed line-like structures [1, page 105]

$$\begin{bmatrix} S_{qz}(\omega) \\ S_{q\theta}(\omega) \end{bmatrix} = \frac{\left(\frac{1}{2}\rho V^2\right)^2}{\sqrt{\pi} \cdot \omega_s} \cdot \begin{bmatrix} \frac{(B \cdot \hat{\sigma}_{qz})^2}{b_z} \cdot \exp\left\{-\left(\frac{1 - \omega/\omega_s}{b_z}\right)^2\right\} \\ \frac{(B^2 \cdot \hat{\sigma}_{q\theta})^2}{b_\theta} \cdot \exp\left\{-\left(\frac{1 - \omega/\omega_s}{b_\theta}\right)^2\right\} \end{bmatrix} \quad (1.50)$$

and an accompanying normalized co-spectrum

$$\hat{C}_{O_{qmz}}(\Delta x) = \cos\left(\frac{2}{3}\frac{\Delta x}{\lambda D}\right) \cdot \exp\left\{-\left(\frac{\Delta x}{3\lambda D}\right)^2\right\} \quad (1.51)$$

where $\hat{\sigma}_{qm}$, $m = z$ or θ , is the nondimensional root mean square lift or torsion coefficient, b_m is the nondimensional load spectrum band width parameter, λ is the nondimensional coherence length scale and $\Delta x (= \Delta y_f)$ is the separation along the span. It may be shown that the integral of the co-spectrum may be approximated [1, page 106]

$$\int_0^\infty \hat{C}_{O_{qm}}(\Delta x) d(\Delta x) \approx \lambda D \quad (1.52)$$

Vickery & Basu have also suggested the aerodynamic damping and stiffness matrices when the only motion induced loading effect of the structure is from vortex shedding [1, page 106]

$$\mathbf{C}_{ae} \approx \frac{\rho B^2}{2} \omega_i(V) \begin{bmatrix} 0 & 0 & 0 \\ 0 & K_{az} \left[1 - \left(\frac{\sigma_{rz}}{a_z D}\right)^2\right] & 0 \\ 0 & 0 & B^2 K_{a\theta} \left[1 - \left(\frac{\sigma_{r\theta}}{a_\theta}\right)^2\right] \end{bmatrix} \quad \text{and} \quad \mathbf{K}_{ae} \approx 0 \quad (1.53)$$

where K_{am} , $m = z$ or θ , is the velocity dependent damping coefficients, and a_m is a quantity associated with the self-limiting characteristic of vortex shedding.

1.5 Response Calculations

In this part the background theory and assumptions for the calculation of the displacement of line-like structures exposed to a turbulent wind field are shown. In structural engineering it is the maximum displacements that are of interest. As the displacements are assumed to depend linearly on the wind velocity which is assumed to have a Gaussian probability distribution, the maximum displacement at the point x_r along the bridge span is the sum of the mean displacement and a peak factor times the Gaussian standard deviation

$$r_{max}(x_r) = \bar{r}(x_r) + k_p \cdot \sigma_r(x_r) \quad (1.54)$$

The definition of the peak factor k_p is shown in section 1.2.1. The derivation of the mean value $\bar{r}(x_r)$ can be performed from straight-forward static equilibrium, and is not considered a part of this report. The standard deviation $\sigma_r(x_r)$ may be found from modal frequency domain calculations presented in the following sections. The steps include expressing the wind load by its auto spectral density and using this to find the response spectrum of the structure, which can be integrated over in order to find the variance and standard deviation.

1.5.1 Dynamic Equilibrium and Frequency Response Function

If the eigenfrequencies are well spaced out on the frequency axis the coupling between the different modes may be neglected. If the centroid and shear center coincide, or nearly coincide, each of the mode shapes will only include one single component, either in y-, z- or θ -direction. This indicates that the total response in each direction can be found by simply summarizing the response of each mode with a component in the considered direction. The following is based on the assumption of uncoupled and single component modes.

A dynamic system with an arbitrary eigenmode $\phi_i(x)$ with eigenfrequency ω_i , damping coefficient ζ_i and distributed mass m_i , exposed to a dynamic load q , will render a single mode response of $r_i(x, t) = \phi_i(x) \cdot \eta_i(t)$ and the modal dynamic equilibrium

$$\tilde{M}_i \cdot \ddot{\eta}_i(t) + \tilde{C}_i \cdot \dot{\eta}_i(t) + \tilde{K}_i \cdot \eta_i(t) = \tilde{Q}_i(t) + \tilde{Q}_{ae_i}(t, \eta_i, \dot{\eta}_i, \ddot{\eta}_i) \quad (1.55)$$

where

$$\tilde{Q}_{ae_i}(t, \eta_i, \dot{\eta}_i, \ddot{\eta}_i) = \tilde{M}_{ae_i} \cdot \ddot{\eta}_i(t) + \tilde{C}_{ae_i} \cdot \dot{\eta}_i(t) + \tilde{K}_{ae_i} \cdot \eta_i(t) \quad (1.56)$$

and

$$\begin{bmatrix} \tilde{M}_i \\ \tilde{C}_i \\ \tilde{K}_i \\ \tilde{Q}_i(t) \end{bmatrix} = \begin{bmatrix} \int_L \phi_i^2 m dx \\ 2\tilde{M}_i \omega_i \zeta_i \\ \tilde{M}_i \omega_i^2 \\ \int_{L_{exp}} \phi_i q dx \end{bmatrix} \quad (1.57)$$

The motion induced load \tilde{Q}_{ae} is depending on η_i and its derivatives and must be transferred to the left side of equation (1.55). Fourier transformation of η_i and $Q_i(t)$ gives

$$\left[-\left(\tilde{M}_i - \tilde{M}_{ae_i} \right) \cdot \omega^2 + \left(\tilde{C}_i - \tilde{C}_{ae_i} \right) \cdot i\omega + \left(\tilde{K}_i - \tilde{K}_{ae_i} \right) \right] \cdot a_{\eta_i} = a_{\tilde{Q}_i} \quad (1.58)$$

By inserting \tilde{C}_i and \tilde{K}_i from equation (1.57) and dividing both sides on \tilde{K}_i the following is obtained

$$\left[-\left(1 - \frac{\tilde{M}_{ae_i}}{\tilde{M}_i} \right) \cdot \left(\frac{\omega}{\omega_i} \right)^2 + 2i \left(\zeta_i - \frac{\tilde{C}_{ae_i}}{2\omega_i \tilde{M}_i} \right) \cdot \frac{\omega}{\omega_i} + \left(1 - \frac{\tilde{K}_{ae_i}}{\omega_i^2 \tilde{M}_i} \right) \right] a_{\eta_i} = \frac{1}{\tilde{K}_i} \cdot a_{\tilde{Q}_i} \quad (1.59)$$

The function within the square bracket is defined as the inverse of the modal frequency response function $\hat{H}_i(t)$, and accordingly may the Fourier amplitude of $\eta_i(t)$ be expressed by

$$a_{\eta_i} = \frac{\hat{H}_i(\omega)}{\tilde{K}_i} \cdot a_{\tilde{Q}_i} \quad (1.60)$$

The frequency response can be understood as the function that describes how the system will respond to an action.

It is common to introduce the aerodynamic coefficients [1, page 78]

$$\begin{bmatrix} \zeta_{ae_i} \\ \kappa_{ae_i} \end{bmatrix} = \begin{bmatrix} \frac{\tilde{C}_{ae_i}}{2\omega_i \tilde{M}_i} \\ \frac{\tilde{K}_{ae_i}}{\omega_i^2 \tilde{M}_i} \end{bmatrix} \quad (1.61)$$

The aerodynamic mass \tilde{M}_{ae_i} has small impact on the total response of line-like structures and is usually neglected. The following expression of the frequency response function is then obtained

$$\hat{H}_i(\omega) = \left[1 - \kappa_{ae_i} - \left(\frac{\omega}{\omega_i} \right)^2 + 2i \left(\zeta_i - \zeta_{ae_i} \right) \cdot \frac{\omega}{\omega_i} \right]^{-1} \quad (1.62)$$

1.5.2 Response Spectrum

Auto spectral density is described in 1.2.2. The response spectrum at a point x_r along a line-like structure may be found from the single sided auto spectral density presented in equation (1.11) and the relation

$$a_{r_i}(\omega) = \phi_i(x_r) \cdot a_{\eta_i}(\omega) \quad (1.63)$$

Inserting a_{η_i} from equation (1.60) the following expression of the response spectrum is obtained

$$\begin{aligned} S_{r_i}(\omega) &= \lim_{T \rightarrow \infty} \frac{1}{\pi T} (a_{r_i}^* \cdot a_{r_i}) = \phi_i^2(x_r) \lim_{T \rightarrow \infty} \frac{1}{\pi T} (a_{\eta_i}^* \cdot a_{\eta_i}) \\ &= \phi_i^2(x_r) \cdot \lim_{T \rightarrow \infty} \frac{1}{\pi T} \left(\frac{\hat{H}_i^*(\omega)}{\tilde{K}_i} a_{\tilde{Q}_i}^* \cdot \frac{\hat{H}_i(\omega)}{\tilde{K}_i} a_{\tilde{Q}_i} \right) \\ &= \frac{\phi_i^2(x_r)}{\tilde{K}_i^2} |\hat{H}_i(\omega)|^2 \lim_{T \rightarrow \infty} \frac{1}{\pi T} (a_{\tilde{Q}_i}^* \cdot a_{\tilde{Q}_i}) = \frac{\phi_i^2(x_r)}{\tilde{K}_i^2} |\hat{H}_i(\omega)|^2 \cdot S_{\tilde{Q}_i}(\omega) \end{aligned} \quad (1.64)$$

where $S_{\tilde{Q}_i}(\omega)$ describes the spectral density of the modal wind load, $\tilde{Q}_i(t) = \int_{L_{eksp}} \phi_i(x) \cdot q_i(x, t) dx$.

The following two sections describe the derivation of respectively buffeting and vortex shedding load spectrum, and how to find the response of each of the two phenomena using the equations above.

1.5.3 Buffeting Response

The buffeting response spectrum for a single mode ϕ_i may be found from equation (1.64), with \tilde{Q}_i from equation (1.57) and $a_{q_i}(\omega)$ equal to the Fourier amplitude of the dynamic buffeting load $\mathbf{q} = \mathbf{B}_q \cdot \mathbf{v}$, where \mathbf{B}_q is given in equation (1.46). It is shown below how to find the expression of the standard deviation of the response of an arbitrary mode in y-direction, the same principles are valid for the response in z- and θ -direction.

The load spectrum of the buffeting wind load in y-direction is given as

$$\begin{aligned}
S_{\tilde{Q}_y}(\omega) &= \lim_{T \rightarrow \infty} \frac{1}{\pi T} (a_{\tilde{Q}_y}^* \cdot a_{\tilde{Q}_y}) = \lim_{T \rightarrow \infty} \frac{1}{\pi T} \left\{ \int_{L_{exp}} \phi_y \cdot a_{q_y}^* dx \right\} \cdot \left\{ \int_{L_{exp}} \phi_y \cdot a_{q_y} dx \right\} \\
&= \left(\frac{\rho V B}{2} \right)^2 \lim_{T \rightarrow \infty} \frac{1}{\pi T} \left\{ \int_{L_{exp}} \phi_y \left[2 \frac{D}{B} \bar{C}_D a_u^* + \left(\frac{D}{B} C'_D - \bar{C}_L \right) a_w^* \right] dx \right\} \\
&\quad \cdot \left\{ \int_{L_{exp}} \phi_y \left[2 \frac{D}{B} \bar{C}_D a_u + \left(\frac{D}{B} C'_D - \bar{C}_L \right) a_w \right] dx \right\}
\end{aligned} \tag{1.65}$$

The integrals may be written into a double integral. Assuming that the cross spectrum between the different flow components are negligible the following is obtained

$$\begin{aligned}
S_{\tilde{Q}_y}(\omega) &= \left(\frac{\rho V B}{2} \right)^2 \iint_{L_{exp}} \phi_y(x_1) \cdot \phi_y(x_2) \cdot \left\{ \left(2 \frac{D}{B} \bar{C}_D \right)^2 S_{uu}(\Delta x, \omega) \right. \\
&\quad \left. + \left(\frac{D}{B} C'_D - \bar{C}_L \right)^2 S_{ww}(\Delta x, \omega) \right\} dx_1 dx_2
\end{aligned} \tag{1.66}$$

The real value of the cross spectrum is defined in equation (1.19). It is common to introduce the standard deviation of the turbulent wind, defined in section 1.3.2, by multiplying the equation with $\frac{V^2}{\sigma_n^2 / I_n^2} = 1$. Inserting this in the equation renders

$$\begin{aligned}
S_{\tilde{Q}_y}(\omega) &= \left(\frac{\rho V^2 B}{2} \right)^2 \iint_{L_{exp}} \phi(x_1) \cdot \phi(x_2) \cdot \left\{ \left[2 \frac{D}{B} \bar{C}_D I_u \right]^2 \hat{C}_{ouu}(\Delta x, \omega) \cdot \frac{S_u(\omega)}{\sigma_u^2} \right. \\
&\quad \left. + \left[\left(\frac{D}{B} C'_D - \bar{C}_L \right) I_w \right]^2 \hat{C}_{oww}(\Delta x, \omega) \cdot \frac{S_w(\omega)}{\sigma_w^2} \right\} dx_1 dx_2 \\
&= \left[\frac{\rho V^2 B}{2} J_y(\omega) \right]^2
\end{aligned} \tag{1.67}$$

where $\frac{S_n(\omega)}{\sigma_n^2}$, $n = u$ or w , may be found from Kaimal's auto spectral density in equation (1.32), and the so-called joint acceptance function, $J_y^2(\omega)$, is

$$\begin{aligned}
J_y^2(\omega) &= \iint_{L_{exp}} \phi_y(x_1) \cdot \phi_y(x_2) \cdot \left\{ \left[2 \frac{D}{B} \bar{C}_D I_u \right]^2 \hat{C}_{ouu}(\Delta x, \omega) \cdot \frac{S_u(\omega)}{\sigma_u^2} \right. \\
&\quad \left. + \left[\left(\frac{D}{B} C'_D - \bar{C}_L \right) I_w \right]^2 \hat{C}_{oww}(\Delta x, \omega) \cdot \frac{S_w(\omega)}{\sigma_w^2} \right\} dx_1 dx_2
\end{aligned} \tag{1.68}$$

The joint acceptance can be understood as the statistically averaging of the influence of the loads over the length of the line-like structure.

As described in section 1.2.2 the variation may be found by integrating over the response spectrum, presented in equation (1.64). Thus may the variation of the response of an arbitrary mode in y -direction be given as

$$\begin{aligned}\sigma_{r_y}^2(x_r) &= \int_0^\infty S_r(x_r, \omega) d\omega = \int_0^\infty \frac{\phi_y^2(x_r)}{\tilde{K}_y^2} \cdot |\hat{H}_y(\omega)|^2 \cdot S_{\tilde{Q}_y}(\omega) d\omega \\ &= \frac{\phi_y^2(x_r)}{\tilde{K}_y^2} \int_0^\infty |\hat{H}_y(\omega)|^2 \cdot \left[\frac{\rho V^2 B}{2} J_y(\omega) \right]^2 d\omega\end{aligned}\quad (1.69)$$

It is common to normalize the joint acceptance function

$$\hat{J}_y^2(\omega) = J_y^2(\omega) / \left(\int_L \phi_y^2 dx \right)^2 \quad (1.70)$$

By introducing this and the relation $\tilde{K}_y = \tilde{M}_y \omega_y^2 = \tilde{m}_y \omega_y^2 \int_L \phi_y^2 dx$, where \tilde{m}_y is the modally equivalent distributed mass, and also taking the square root of the variation, the following expression of the standard deviation is obtained

$$\sigma_{r_y}(x_r) = |\phi_y(x_r)| \cdot \frac{\rho V^2 B}{2 \tilde{m}_y \omega_y^2} \cdot \left[\int_0^\infty |\hat{H}_y(\omega)|^2 \cdot \hat{J}_y^2(\omega) d\omega \right]^{1/2} \quad (1.71)$$

As the modes are assumed uncoupled and including only one component each, the total standard deviation of the response in y -direction may be found by summing the standard deviation of each of the modes with components in y -direction

$$\sigma_{r_y}(x_r) = \sum_{i_y} \sigma_{r_{i_y}}(x_r) \quad (1.72)$$

By the same principles it can be shown that the standard deviations of a single mode in z - or θ -direction are

$$\sigma_{r_z}(x_r) = |\phi_z(x_r)| \cdot \frac{\rho V^2 B}{2 \tilde{m}_z \omega_z^2} \cdot \left[\int_0^\infty |\hat{H}_z(\omega)|^2 \cdot \hat{J}_z^2(\omega) d\omega \right]^{1/2} \quad (1.73)$$

$$\sigma_{r_\theta}(x_r) = |\phi_\theta(x_r)| \cdot \frac{\rho V^2 B^2}{2 \tilde{m}_\theta \omega_\theta^2} \cdot \left[\int_0^\infty |\hat{H}_\theta(\omega)|^2 \cdot \hat{J}_\theta^2(\omega) d\omega \right]^{1/2} \quad (1.74)$$

where the normalized joint acceptance functions are given as

$$\begin{aligned} \hat{J}_z^2(\omega) = & \frac{1}{(\int_L \phi_z^2 dx)^2} \cdot \iint_{L_{exp}} \phi_z(x_1) \cdot \phi_z(x_2) \cdot \left\{ [2\bar{C}_L I_u]^2 \hat{C}_{ouu}(\Delta x, \omega) \cdot \frac{S_u(\omega)}{\sigma_u^2} \right. \\ & \left. + \left[\left(C'_L + \frac{D}{B} \bar{C}_D \right) I_w \right]^2 \hat{C}_{oww}(\Delta x, \omega) \cdot \frac{S_w(\omega)}{\sigma_w^2} \right\} dx_1 dx_2 \end{aligned} \quad (1.75)$$

$$\begin{aligned} \hat{J}_\theta^2(\omega) = & \frac{1}{(\int_L \phi_\theta^2 dx)^2} \cdot \iint_{L_{exp}} \phi_\theta(x_1) \cdot \phi_\theta(x_2) \cdot \left\{ [2\bar{C}_M I_u]^2 \hat{C}_{ouu}(\Delta x, \omega) \cdot \frac{S_u(\omega)}{\sigma_u^2} \right. \\ & \left. + [C'_M I_w]^2 \hat{C}_{oww}(\Delta x, \omega) \cdot \frac{S_w(\omega)}{\sigma_w^2} \right\} dx_1 dx_2 \end{aligned} \quad (1.76)$$

1.5.4 Vortex Shedding Response

The vortex shedding load spectrum of an arbitrary mode ϕ_i in z - or θ -direction may be derived from the definition of spectral density in equation (1.11)

$$S_{\tilde{Q}_i}(\omega) = \lim_{T \rightarrow \infty} \frac{1}{\pi T} \left(a_{\tilde{Q}_i}^* \cdot a_{\tilde{Q}_i} \right) = \lim_{T \rightarrow \infty} \frac{1}{\pi T} \left\{ \int_{L_{exp}} \phi_i \cdot a_{q_i}^* dx \right\} \cdot \left\{ \int_{L_{exp}} \phi_i \cdot a_{q_i} dx \right\} \quad (1.77)$$

The expression may be written into a double integral, and the cross spectrum between two realizations of q_i may be replaced by the single point load spectrum multiplied with the normalized co-spectrum as shown in equation (1.19)

$$\begin{aligned} S_{\tilde{Q}_i}(\omega) &= \iint_{L_{exp}} \phi_i(x_1) \left\{ \lim_{T \rightarrow \infty} \frac{1}{\pi T} a_{q_i}^* \cdot a_{q_i} \right\} \phi_i(x_2) dx_1 dx_2 \\ &= \iint_{L_{exp}} \phi_i(x_1) \cdot S_{q_i q_i}(\Delta x, \omega) \cdot \phi_i(x_2) dx_1 dx_2 \\ &= S_{q_i}(\omega) \iint_{L_{exp}} \phi_i(x_1) \cdot \hat{C}_{oq_i}(\Delta x) \cdot \phi_i(x_2) dx_1 dx_2 \end{aligned} \quad (1.78)$$

The normalized co-spectrum of vortex shedding is discussed in section 1.4.2. Dyrbye & Hansen [2] suggest writing the double integral into two line integrals

$$S_{\tilde{Q}_i}(\omega) = S_{q_i}(\omega) \int_{L_{exp}} \left[2 \int_0^{L_{exp} - \Delta x} \phi_i(x) \cdot \phi_i(x + \Delta x) dx \right] \hat{C}_{oq_i}(\Delta x) d\Delta x \quad (1.79)$$

The integral length scale of the vortices is approximately λD , see equation (1.52). It is a reasonable assumption that this value is small compared to L_{exp} and thus may the load spectrum be approximated

$$S_{\tilde{Q}_i}(\omega) \approx 2\lambda D \cdot S_{q_i}(\omega) \cdot \int_{L_{exp}} \phi_i^2(x) dx \quad (1.80)$$

Because vortex shedding induced dynamic response usually is largely resonant and narrow-banded, it is sufficient to only consider the resonant frequency [1, page 146]. From this assumption and equation (1.7) and (1.64) the expression of the variance of the response in position x_r may be approximated

$$\begin{aligned} \sigma_{r_i}^2(x_r) &= \int_0^\infty S_r(x_r, \omega) d\omega = \frac{\phi_i^2(x_r)}{\tilde{K}_i^2} \cdot \int_0^\infty |\hat{H}_i(\omega)|^2 \cdot S_{\tilde{Q}_i}(\omega) d\omega \\ &\approx \frac{\phi_i^2(x_r)}{\tilde{K}_i^2} \left\{ \int_0^\infty |\hat{H}_i(\omega)|^2 d\omega \right\} \cdot S_{\tilde{Q}_i}(\omega_i) \end{aligned} \quad (1.81)$$

The integration of the frequency response, see equation (1.62), is presented several places in the literature, for instance in D. E. Newland [3]

$$I = \int_{-\infty}^\infty |H_i(\omega)|^2 d\omega = \frac{\pi\omega_i}{2(1 - \kappa_{ae_i})(\zeta_i - \zeta_{ae_i})} \quad (1.82)$$

where

$$\zeta_{ae_i} = \frac{\tilde{C}_{ae_i}}{2\omega_i \tilde{M}_i} = \frac{1}{2\omega_i \tilde{m}_i} \cdot \frac{\int_{L_{exp}} C_{ae_i} \cdot \phi_i^2(x) dx}{\int_L \phi_i^2(x) dx} \quad (1.83)$$

C_{ae_i} is defined in equation (1.53), and i is an arbitrary mode in z - or θ -direction. κ_{ae_i} must be zero because of the assumption made in section 1.4.2 of $\mathbf{K}_{ae} = \mathbf{0}$.

This renders the following expression of the variance of the response

$$\sigma_{r_i}^2 = \frac{\phi_i^2(x_r)}{\tilde{K}_i^2} \cdot \frac{1}{2} I \cdot S_{\tilde{Q}_i}(\omega_i) = \frac{\phi_i^2(x_r)}{\tilde{K}_i^2} \cdot \frac{\pi\omega_i}{4(\zeta_i - \zeta_{ae_i})} \cdot S_{\tilde{Q}_i}(\omega_i) \quad (1.84)$$

Inserting $S_{\tilde{Q}_i}$ from equation (1.80), introducing $\tilde{K}_i = \tilde{M}_i\omega_i^2 = \tilde{m}_i\omega_i^2 \int_L \phi_i^2 dx$ and taking the square root of the variance give the expression of the standard deviation of the vortex shedding induced response

$$\sigma_{r_i}(x_r) = \sqrt{\frac{\phi_i^2(x_r)}{(\tilde{m}_i \omega_i^2 \int_L \phi_i^2(x) dx)^2} \cdot \frac{\pi \omega_i}{4(\zeta_i - \zeta_{ae_i})} \cdot \left\{ 2\lambda D S_{q_i}(\omega_i) \int_{L_{exp}} \phi_i^2(x) dx \right\}} \quad (1.85)$$

By inserting S_{q_i} from equation (1.50) and introducing the resonance mean wind velocity $V_{R_i} = D\omega_i/2\pi St$, the standard deviation of the displacement of an arbitrary mode in z - or θ -direction is obtained

$$\begin{aligned} \sigma_{r_z}(x_r) = & \frac{|\phi_z(x_r)|}{2^{7/2}\pi^{7/4}} \cdot \frac{\rho B D^2}{\tilde{m}_z} \cdot \frac{\hat{\sigma}_{q_z}}{St^2} \cdot \left[\frac{\lambda}{b_z \cdot (\zeta_z - \zeta_{ae_z})} \right]^{1/2} \cdot \frac{\left(D \int_{L_{exp}} \phi_z^2(x) dx \right)^{1/2}}{\int_L \phi_z^2(x) dx} \\ & \cdot \left(\frac{V}{V_R} \right)^{3/2} \cdot \exp \left[-\frac{1}{2} \left(\frac{1 - V_R/V}{b_z} \right)^2 \right] \end{aligned} \quad (1.86)$$

$$\begin{aligned} \sigma_{r_\theta}(x_r) = & \frac{|\phi_\theta(x_r)|}{2^{7/2}\pi^{7/4}} \cdot \frac{\rho B^2 D^2}{\tilde{m}_\theta} \cdot \frac{\hat{\sigma}_{q_\theta}}{St^2} \cdot \left[\frac{\lambda}{b_\theta \cdot (\zeta_\theta - \zeta_{ae_\theta})} \right]^{1/2} \cdot \frac{\left(D \int_{L_{exp}} \phi_\theta^2(x) dx \right)^{1/2}}{\int_L \phi_\theta^2(x) dx} \\ & \cdot \left(\frac{V}{V_R} \right)^{3/2} \cdot \exp \left[-\frac{1}{2} \left(\frac{1 - V_R/V}{b_\theta} \right)^2 \right] \end{aligned} \quad (1.87)$$

where

$$\zeta_{ae_z} = \frac{\rho B^2}{4\tilde{m}_z} \cdot K_{a_z} \cdot \left[1 - \left(\frac{\sigma_{r_z}}{a_z D} \right)^2 \right] \cdot \frac{\int_{L_{exp}} \phi_z^2(x) dx}{\int_L \phi_z^2(x) dx} \quad (1.88)$$

$$\zeta_{ae_\theta} = \frac{\rho B^4}{4\tilde{m}_\theta} \cdot K_{a_\theta} \cdot \left[1 - \left(\frac{\sigma_{r_\theta}}{a_\theta} \right)^2 \right] \cdot \frac{\int_{L_{exp}} \phi_\theta^2(x) dx}{\int_L \phi_\theta^2(x) dx} \quad (1.89)$$

Inserting for ζ_{ae_z} into equation (1.86) or ζ_{ae_θ} into equation (1.87), results in a fourth degree polynomial on the following form

$$\hat{\sigma}_{r_m}^4 - (1 - \hat{\zeta}_m) \hat{\sigma}_{r_m}^2 - \hat{\beta}_m^2 = 0 \quad (1.90)$$

with the solution

$$\hat{\sigma}_{r_m} = \left\{ \frac{1 - \hat{\zeta}_m}{2} + \left[\left(\frac{1 - \hat{\zeta}_m}{2} \right)^2 + \hat{\beta}_m^2 \right]^{1/2} \right\}^{1/2} \quad (1.91)$$

where $m = z$ or θ and

$$\hat{\sigma}_{r_z} = \frac{\sigma_{r_z}}{a_z D} \quad (1.92)$$

$$\hat{\zeta}_z = \frac{4\tilde{m}_z \zeta_z}{\rho B^2 K_{a_z}} \cdot \frac{\int_L \phi_z^2 dx}{\int_{L_{exp}} \phi_z^2 dx} \quad (1.93)$$

$$\hat{\beta}_z = \frac{|\phi_z(x_r)|}{2^{5/2} \pi^{7/4}} \cdot \left(\frac{\rho D^3 \lambda}{\tilde{m}_z b_z K_{a_z} \int_L \phi_z^2 dx} \right)^{1/2} \cdot \frac{\hat{\sigma}_{q_z}}{St^2 a_z} \cdot \left(\frac{V}{V_R} \right)^{3/2} \exp \left[-\frac{1}{2} \left(\frac{1 - V_R/V}{b_z} \right)^2 \right] \quad (1.94)$$

$$\hat{\sigma}_{r_\theta} = \frac{\sigma_{r_\theta}}{a_z} \quad (1.95)$$

$$\hat{\zeta}_\theta = \frac{4\tilde{m}_\theta \zeta_\theta}{\rho B^4 K_{a_\theta}} \cdot \frac{\int_L \phi_\theta^2 dx}{\int_{L_{exp}} \phi_\theta^2 dx} \quad (1.96)$$

$$\hat{\beta}_\theta = \frac{|\phi_\theta(x_r)|}{2^{5/2} \pi^{7/4}} \cdot \left(\frac{\rho D^5 \lambda}{\tilde{m}_\theta b_\theta K_{a_\theta} \int_L \phi_\theta^2 dx} \right)^{1/2} \cdot \frac{\hat{\sigma}_{q_\theta}}{St^2 a_\theta} \cdot \left(\frac{V}{V_R} \right)^{3/2} \exp \left[-\frac{1}{2} \left(\frac{1 - V_R/V}{b_\theta} \right)^2 \right] \quad (1.97)$$

The response from vortex shedding is usually significant for resonant mean wind velocities, and small when the wind velocity is not around these values.

1.6 Determination of Cross Sectional Forces

This section focuses on the determination of the cross sectional forces of a line-like structure exposed to a turbulent wind field. It is assumed linear elastic material behavior and a linear relationship between the wind flow and the load effects, and as the wind flow is assumed a stochastic process with Gaussian probability distribution the cross sectional maximum force at a point x_r along the structure may also be described by its mean value and standard deviation

$$F_{max}(x_r) = \bar{F}(x_r) + k_p \cdot \sigma_F(x_r) \quad (1.98)$$

where k_p is the peak factor as described in section 1.2.1.

The forces may be calculated directly from the derivatives of the eigenmodes, but as these eigenmodes usually are only an approximation of the actual structural behavior

their second and third order derivatives may be inaccurate. It is therefore common to divide the variance of the cross sectional forces into a background- and a resonant part, as shown in figure 1.7.

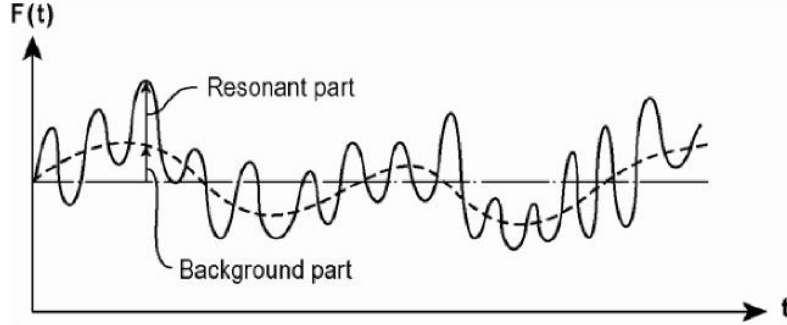


Figure 1.7: The standard deviation of a cross sectional force $F(t)$ divided into a background and a resonant part [1, page 159]

The maximum value of $F(x_r)$ may then be given as

$$F_{max}(x_r) = \bar{F}(x_r) + k_p \cdot \sqrt{\sigma_{F_B}^2(x_r) + \sigma_{F_R}^2(x_r)} \quad (1.99)$$

The mean value is obtained from static calculations, which is considered trivial and therefore not included in this report. The background part may be found from quasi-static considerations and the resonant part by using the derivatives of the resonant displacements.

1.6.1 Background Part

The background part is the slowly varying part of the response, see figure 1.7, which means that inertia forces may be disregarded such that only static considerations are needed, hence the characterization quasi-static. A simplified approach based on so-called influence functions are presented below.

The distributed buffeting wind load on a line-like structure when the mean part and the motion induced contributions are disregarded is $\mathbf{q} = \mathbf{B}_q \cdot \mathbf{v}$, see equation (1.42), where \mathbf{B}_q is given in equation (1.46).

The load in each direction may be treated separately when assuming single component modes. If the structure is fairly uncomplicated and static influence functions are easily obtained the cross sectional stress resultants due to the background part of the response may be given as [1, page 164]

$$\begin{bmatrix} M_x(x_r, t) \\ M_z(x_r, t) \\ M_y(x_r, t) \\ V_y(x_r, t) \\ V_z(x_r, t) \end{bmatrix}_B = \begin{bmatrix} \int_{L_{exp}} G_{M_x}(x) \cdot q_\theta(x, t) \\ \int_{L_{exp}} G_{M_z}(x) \cdot q_y(x, t) \\ \int_{L_{exp}} G_{M_y}(x) \cdot q_z(x, t) \\ \int_{L_{exp}} G_{V_y}(x) \cdot q_y(x, t) \\ \int_{L_{exp}} G_{V_z}(x) \cdot q_z(x, t) \end{bmatrix} \quad (1.100)$$

whereas $M_{x_B}(x_r, t) \neq 0$ for a mode containing only the θ -component, $M_{z_B}(x_r, t)$ and $V_{y_B}(x_r, t) \neq 0$ for a mode containing only the y-component and $M_{y_B}(x_r, t)$ and $V_{z_B}(x_r, t) \neq 0$ for a mode containing only the z-component. $G_F(x)$, where $F = M_x, M_z, M_y, V_y$ or V_z , is the relevant influence function, depending on the static system.

Using $\sigma_{M_{z_B}}^2$ as an example, inserting for the buffeting point load $q_y(x, t)$ from equation (1.42) and (1.46) gives

$$M_{z_B}(x_r, t) = \int_{L_{exp}} G_{M_z}(x) \cdot \frac{\rho V B}{2} \left[2 \frac{D}{B} \bar{C}_D \cdot u(x, t) + \left(\frac{D}{B} C'_D - \bar{C}_L \right) \cdot w(x, t) \right] dx \quad (1.101)$$

The variance of M_{z_B} is by definition [1, page 165]

$$\begin{aligned} \sigma_{M_{z_B}}^2 &= E \left[\{M_{z_B}(x_r, t)\}^2 \right] = E \left[\left\{ \int_{L_{exp}} G_{M_z}(x) \cdot q_y(x, t) dx \right\}^2 \right] \\ &= \iint_{L_{exp}} G_{M_z}(x_1) \cdot G_{M_z}(x_2) \cdot E[q_y(x_1, t) \cdot q_y(x_2, t)] dx_1 dx_2 \end{aligned} \quad (1.102)$$

As usual the cross covariance between different components is neglected. The cross covariance between the same velocity components may be found from the definition of the auto cross covariance coefficient presented in equation (1.16)

$$\begin{aligned} E[u(x_1, t) \cdot u(x_2, t)] &= \sigma_u^2 \cdot \rho_{uu}(\Delta x) \\ E[w(x_1, t) \cdot w(x_2, t)] &= \sigma_w^2 \cdot \rho_{ww}(\Delta x) \end{aligned} \quad (1.103)$$

where $\sigma_n = I_n V$, see equation (1.23), and an approximation of ρ_{nn} is presented in equation (1.29), $n = u$ or w .

The variance is accordingly

$$\sigma_{M_z B}^2 = \left(\frac{\rho V^2 B}{2} \right)^2 \iint_{Lexp} G_{M_z}(x_1) \cdot G_{M_z}(x_2) \cdot \left[\left(2 \frac{D}{B} \bar{C}_D I_u \right)^2 \rho_{uu}(\Delta x) + \left[\left(\frac{D}{B} C'_D - \bar{C}_L \right) I_w \right]^2 \rho_{ww}(\Delta x) \right] dx_1 dx_2 \quad (1.104)$$

The same steps may be used to find the variance of the other cross sectional stress resultants due to the background part of the response

$$\sigma_{M_x B}^2 = \left(\frac{\rho V^2 B}{2} \right)^2 \iint_{Lexp} G_{M_x}(x_1) \cdot G_{M_x}(x_2) \cdot B^2 \left[\left(2 \bar{C}_M I_u \right)^2 \rho_{uu}(\Delta x) + [C'_M I_w]^2 \rho_{ww}(\Delta x) \right] dx_1 dx_2 \quad (1.105)$$

$$\sigma_{M_y B}^2 = \left(\frac{\rho V^2 B}{2} \right)^2 \iint_{Lexp} G_{M_y}(x_1) \cdot G_{M_y}(x_2) \cdot \left[\left(2 \bar{C}_L I_u \right)^2 \rho_{uu}(\Delta x) + \left[\left(C'_L + \frac{D}{B} \bar{C}_D \right) I_w \right]^2 \rho_{ww}(\Delta x) \right] dx_1 dx_2 \quad (1.106)$$

$$\sigma_{V_y B}^2 = \left(\frac{\rho V^2 B}{2} \right)^2 \iint_{Lexp} G_{V_y}(x_1) \cdot G_{V_y}(x_2) \cdot \left[\left(2 \frac{D}{B} \bar{C}_D I_u \right)^2 \rho_{uu}(\Delta x) + \left[\left(\frac{D}{B} C'_D - \bar{C}_L \right) I_w \right]^2 \rho_{ww}(\Delta x) \right] dx_1 dx_2 \quad (1.107)$$

$$\sigma_{V_z B}^2 = \left(\frac{\rho V^2 B}{2} \right)^2 \iint_{Lexp} G_{V_z}(x_1) \cdot G_{V_z}(x_2) \cdot \left[\left(2 \bar{C}_L I_u \right)^2 \rho_{uu}(\Delta x) + \left[\left(C'_L + \frac{D}{B} \bar{C}_D \right) I_w \right]^2 \rho_{ww}(\Delta x) \right] dx_1 dx_2 \quad (1.108)$$

The influence function will depend on the static system. For instance will a cantilever when looking at moment around the z-axis have the influence function $G_{M_z} = \frac{x^2}{2}$.

1.6.2 Resonant Part

The resonant part of the standard deviation of the response may as mentioned be found by the derivatives of the displacements. The relationships between the cross sectional forces and the derivatives of the displacements are given by [1, page 183]

$$\mathbf{F}(x_r, t) = \begin{bmatrix} V_y(x_r, t) \\ V_z(x_r, t) \\ M_x(x_r, t) \\ M_y(x_r, t) \\ M_z(x_r, t) \end{bmatrix} = \begin{bmatrix} -EI_z \cdot r_y'''(x_r, t) \\ -EI_y \cdot r_z'''(x_r, t) \\ GI_t \cdot r_\theta'(x_r, t) - EI_w \cdot r_\theta'''(x_r, t) \\ -EI_y \cdot r_z''(x_r, t) \\ EI_z \cdot r_y''(x_r, t) \end{bmatrix} \quad (1.109)$$

The standard deviations of the resonant part are usually found by calculations in the frequency domain. The spectral density of $\mathbf{F}(x_r, t)$ may be derived from the definition of spectral density in equation (1.11)

$$\mathbf{S}_F(x_r, \omega) = \lim_{T \rightarrow \infty} \frac{1}{\pi T} \cdot \mathbf{a}_F^* \cdot \mathbf{a}_F \quad (1.110)$$

Assuming single component and uncoupled modes the different cross sectional forces for each mode may be calculated separately. The derivation of the moment around the y-axis for an arbitrary mode in z-direction is shown below, but the procedure is valid for shear stress, moment around the z-axis and torsional moment as well.

The spectral density becomes

$$\begin{aligned} S_{M_y}(x_r, \omega) &= \lim_{T \rightarrow \infty} \frac{1}{\pi T} \cdot \left\{ EI_y \cdot \phi_z''(x_r) a_\eta^* \right\} \cdot \left\{ EI_y \cdot \phi_z''(x_r) a_\eta \right\} \\ &= [EI_y \cdot \phi_z''(x_r)]^2 \lim_{T \rightarrow \infty} \frac{1}{\pi T} (a_\eta^* \cdot a_\eta) \end{aligned} \quad (1.111)$$

Inserting a_η from equation (1.60) renders

$$\begin{aligned} S_{M_y}(x_r, \omega) &= [EI_y \cdot \phi_z''(x_r)]^2 \lim_{T \rightarrow \infty} \frac{1}{\pi T} \left\{ \frac{\hat{H}^*(\omega)}{\tilde{K}_z} \cdot a_{\tilde{Q}}^* \right\} \cdot \left\{ \frac{\hat{H}(\omega)}{\tilde{K}_z} \cdot a_{\tilde{Q}} \right\} \\ &= \left[\frac{EI_y \cdot \phi_z''(x_r)}{\tilde{K}_z} \right]^2 \cdot |\hat{H}(\omega)|^2 \cdot S_{\tilde{Q}_R} \end{aligned} \quad (1.112)$$

where $S_{\tilde{Q}_R}$ is the resonant part of the load spectrum, similar to $S_{\tilde{Q}_z}(\omega)$ as presented in section 1.5.3 for buffeting wind loads and in section 1.5.4 for vortex shedding loads, but with $\omega = \omega_z$.

The variance may be calculated by equation (1.7), rendering

$$\sigma_{M_{yR}}^2(x_r) = \int_0^\infty S_{M_y}(x_r, \omega) d\omega = \left[\frac{EI_y \cdot \phi_z''(x_r)}{\tilde{K}_z} \right]^2 \cdot \left\{ \int_0^\infty |\hat{H}(\omega)|^2 d\omega \right\} \cdot S_{\tilde{Q}_z}(\omega_z) \quad (1.113)$$

The integration of the frequency response from $-\infty$ to ∞ is shown in equation (1.82). By inserting this, introducing $\tilde{K}_z = \tilde{M}_z \omega_z^2 = \tilde{m}_z \omega_z^2 \int_L \phi_z^2 dx$, and taking the square root of the variance, the standard deviation of the resonant part of the force is obtained

$$\sigma_{M_{yR}}(x_r) = \frac{|EI_y \cdot \phi_z''(x_r)|}{\tilde{m}_z \omega_z^2 \int_L \phi_z^2 dx} \cdot \left[\frac{\pi \omega_z \cdot S_{\tilde{Q}_z}(\omega_z)}{4(1 - \kappa_{aez}) \cdot (\zeta_z - \zeta_{aez})} \right]^{1/2} \quad (1.114)$$

The same procedure may be used to obtain the standard deviations of the resonant part of the force due to eigenmodes in other directions. A single mode containing only the component in y-direction will induce shear forces in y-direction and moment around the z-axis

$$\begin{bmatrix} \sigma_{V_{yR}}(x_r) \\ \sigma_{M_{zR}}(x_r) \end{bmatrix} = \frac{1}{\tilde{m}_y \omega_y^2 \int_L \phi_y^2 dx} \cdot \left[\frac{\pi \omega_y \cdot S_{\tilde{Q}_y}(\omega_y)}{4(1 - \kappa_{ae_y}) \cdot (\zeta_y - \zeta_{ae_y})} \right]^{1/2} \begin{bmatrix} |EI_z \cdot \phi_y'''(x_r)| \\ |EI_z \cdot \phi_y''(x_r)| \end{bmatrix} \quad (1.115)$$

while a single mode containing only the z-component induces shear forces in z-direction and moment about the y-axis

$$\begin{bmatrix} \sigma_{V_{zR}}(x_r) \\ \sigma_{M_{yR}}(x_r) \end{bmatrix} = \frac{1}{\tilde{m}_z \omega_z^2 \int_L \phi_z^2 dx} \cdot \left[\frac{\pi \omega_z \cdot S_{\tilde{Q}_z}(\omega_z)}{4(1 - \kappa_{ae_z}) \cdot (\zeta_z - \zeta_{ae_z})} \right]^{1/2} \begin{bmatrix} |EI_y \cdot \phi_z'''(x_r)| \\ |EI_y \cdot \phi_z''(x_r)| \end{bmatrix} \quad (1.116)$$

and a single mode containing only the θ -component induces torsional moment

$$\sigma_{M_{xR}}(x_r) = \frac{1}{\tilde{m}_\theta \omega_\theta^2 \int_L \phi_\theta^2 dx} \cdot \left[\frac{\pi \omega_\theta \cdot S_{\tilde{Q}_\theta}(\omega_\theta)}{4(1 - \kappa_{ae_\theta}) \cdot (\zeta_\theta - \zeta_{ae_\theta})} \right]^{1/2} |GI_t \cdot \phi_\theta'(x_r) - EI_w \cdot \phi_\theta'''(x_r)| \quad (1.117)$$

where $S_{\tilde{Q}_i}$ is as presented in section 1.5.3 for buffeting wind loads, $i = y, z$ or θ , and in section 1.5.4 for vortex shedding loads, $i = z$ or θ .

1.7 Time Domain Simulations

It is sometimes useful to simulate the variables in the time domain. When dealing with non-linear effects it is a necessity as these are neglected in a frequency domain approach. Time domain simulations are also often used for deciding the peak factor of a process.

The time dependent variable is found by reversing the Fourier transformation described in section 1.2.2. The time series is approximated

$$x(t) = \sum_{k=1}^N c_k \cos(\omega_k t + \phi_k) \quad (1.118)$$

and the amplitude of each harmonic function, c_k , may be found from equation (1.6). Thus is the variable

$$x(t) = \sum_{k=1}^N \sqrt{2 \cdot S_X(\omega_k) \Delta\omega_k} \cdot \cos(\omega_k t + \phi_k) \quad (1.119)$$

where ϕ_k is an arbitrary phase angle between zero and 2π . The variable may be simulated directly from a calculation program where ϕ_k is chosen randomly. The larger N the more accurate results.

2 Calculations

2.1 Introduction

The theory described above shall now be utilized at a concrete example. It has been chosen to perform calculations on Dolmsundet Bridge at its critical construction stage. Dolmsundet Bridge is a rectangular box girder bridge connecting Dolmøya and Hitra in Sør-Trøndelag. It is chosen to construct the bridge by the balanced cantilevered method in order to minimize the temporary work. The construction method has a critical stage at the moment before the cantilevered girders are connected to an adjacent girder or the abutment, because at this point the pillar's bending and torsional moment capacity must endure all wind induced loads on the construction. The bridge is replacing the existing Vettastraumen Bridge and is planned to open in 2015 [4].

It has been developed a computational program in MATLAB in order to find the dynamic response of the cantilever girders in the horizontal and vertical direction due to buffeting and vortex shedding induced loads. The calculations are only performed for the first two eigenmodes, but may easily be expanded to include more modes.

This report will only focus on the calculation of dynamic response, the static response may easily be found from straight forward static considerations. The FE analysis of the bridge is not included in this report. The eigenfrequencies, eigenmodes, mass matrices etc. are adopted from the Norwegian Public Roads Administration's calculations.

2.2 Balanced Cantilever Bridges

Balanced cantilevered bridges are built by sequentially expanding the girder in both directions from a pillar such that the weight on each side compensate for each other. This reduces the need for temporary falsework to a minimum. In order to obtain as light bridge as possible, the height of the cantilevered girders decreases towards the midspan where the bending moment is smallest. Either precast elements are lifted into place, or the concrete are casted in-situ by the use of travelling forms. The latter method is used for the construction of Dolmsundet Bridge.

Figure 2.1 shows the construction of Pierre Pflimlin Bridge, a balanced cantilevered box girder bridge built by using travelling forms and in-situ casting.

At the construction stage just before the cantilevers are connected to either solid ground or an adjacent cantilever, the bridge will be at its most vulnerable against wind loads. The lever arm from the pillar to the tip of the cantilever is long compared to the cross sectional dimensions of the pillar which indicates that even small loads out here will induce large moment and torsional stress in the pillar. The engineers calculating Dolmsundet Bridge have solved this problem by using a temporary support. As this is expensive



Figure 2.1: The construction of Pierre Pfmilin Bridge [5]

and time consuming the possibility of constructing the bridge without the temporary support will be evaluated in this report.

2.3 General Assumptions and Simplifications

A couple of assumptions and simplifications must be made in order to use the theory above directly.

It is assumed linear elastic material and a linear relation between the wind velocity, the displacements and the stress resultants. As the wind velocity is assumed to fit into a Gaussian probability distribution, the displacements and stress resultants are also Gaussian probability distributed. The modes and the displacement components are assumed to be uncoupled such that the total response in each direction may be found by adding up the response of each of the modes in the particular direction. The calculations below only include the two first eigenmodes, as it is assumed that these will represent the major parts of the total response.

The main wind direction is assumed perpendicular to the bridge beam. The entire length of the bridge beam is assumed exposed to buffeting wind such that $L_{exp} = L$, while only the outer half of the cantilevered girders are assumed influenced by vortex shedding. The wind on the pillar is neglected. It is assumed that mean wind velocity is well below any instability limit, and thus, the eigenfrequencies remain the same for all mean wind velocities, i.e. $\omega_i(V) = \omega_i(V = 0)$.

Of simplicity reasons it is used a constant bridge elevation height, z_f . This is further described in section 2.5.1.

For the calculation of vortex shedding induced loads the cross section is assumed to have a constant height, D , see section 2.6.

2.4 Properties of Dolmsundet Bridge

Dolmsundet Bridge is approximately 484 meter long with a main span on 190 meters. Figure 2.2 shows the cross section of the bridge. It is a box girder with varying height, D , from 2.75 at the midspan to 10 meters above the pillars. The width, B , is 11.1 meters. The x -axis is defined in the direction along the bridge span, the z -axis is vertical and the y -axis is in the horizontal along wind direction.

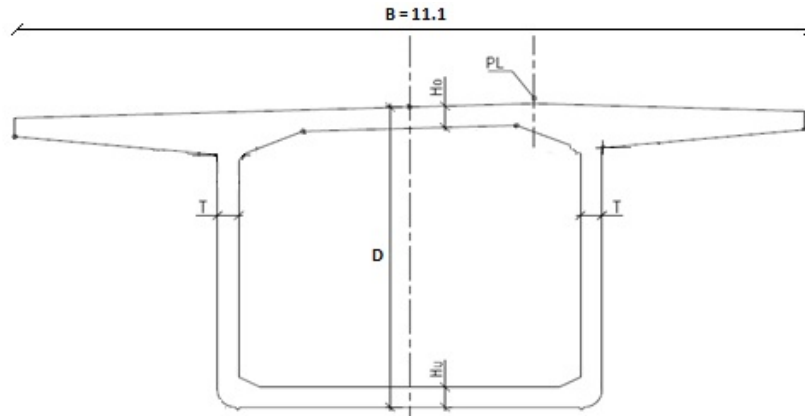


Figure 2.2: The cross section of the bridge beam [6]

The FE analysis of the bridge is performed by the Norwegian Public Roads Administration in the program RM Bridge [7]. A figure that shows the division of the span into elements is presented in appendix A. The worst case regarding wind is when element 106 to 147 are installed and the girder is not yet connected to the abutment. Each element is 4.9 meters long, except number 116, 117 and number 126 to 129. The nodes are defined at the left side of the element so that node 106 are on the far left side of the left cantilever in the critical state and node 148 at the far right side. Figure 2.3 shows a sketch of the construction at the critical stage with relevant dimensions.

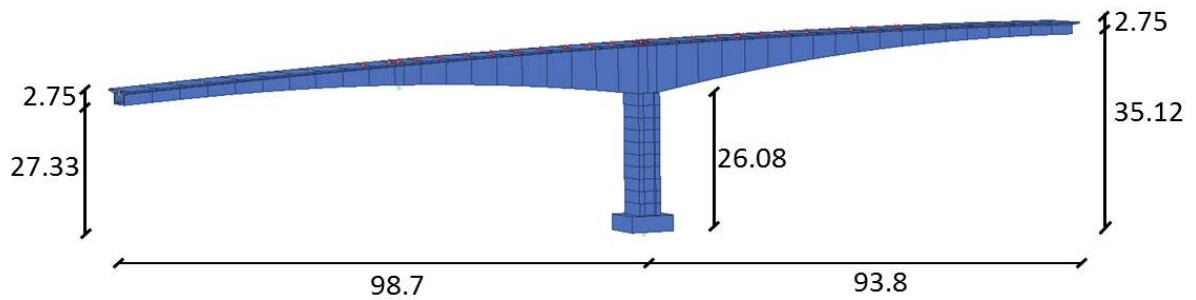


Figure 2.3: Model of Dolmsundet Bridge in the critical construction stage [8]

Figure 2.4 shows the first two eigenmodes of the bridge at this stage. The first one is purely in the horizontal direction, which induces torsional moment in the pillar. The second eigenmode is in the vertical direction and induces bending moment in the pillar. The second mode also includes an along the span displacement, i.e. in x-direction, which is not included in the figure, but will have great impact on the modal mass and also affect the pillar's cross sectional forces.

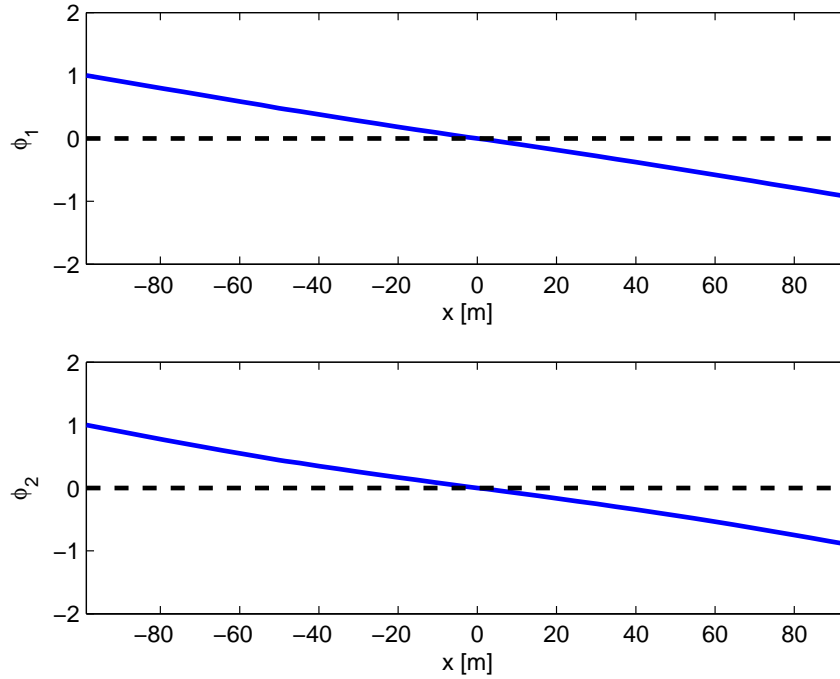


Figure 2.4: The first two eigenmodes of Dolmsundet Bridge in the critical construction stage

The modal properties of the bridge are presented in table 2.1. The modally equivalent distributed masses are calculated from the lumped mass matrix received from the Norwegian Public Roads Administration, whereas $\tilde{m}_1 = \int_L \phi_{1,y}^2 m dx / \int_L \phi_{1,y}^2 dx$ and $\tilde{m}_2 = \int_L (\phi_{2,z}^2 + \phi_{2,x}^2) m dx / \int_L (\phi_{2,z}^2 + \phi_{2,x}^2) dx$.

Eigenmode nr.	$\tilde{m}_i [kg/m]$	$\omega_i [rad/s]$	ζ_i	Direction
1	11526.99	1.401	0.008	Y
2	11762.53	1.687	0.008	Z + X

Table 2.1: Modal properties of the two first eigenmodes [7]

2.5 Buffeting Response Calculations

The response in position x_r along the span may as mentioned be calculated as a sum of the mean displacement and a peak value times the standard deviation

$$r_{max}(x_r) = \bar{r}(x_r) + k_p \cdot \sigma_r(x_r) \quad (2.1)$$

The main concern regarding Dolmsundet Bridge in the construction phase is torsion and moment in the pillar. Thus is the critical r_{max} occurring when $\bar{r}(x_r) = 0$. The standard deviation is found by a frequency domain approach as presented in the theory part. This includes finding the spectral density and the co-spectrum of the turbulent wind, calculating the frequency response and the joint acceptance function, and employ this to calculate the response spectrum which is integrated over in order to find the standard deviation. As the modes are assumed uncoupled the standard deviation of the bridge in y - and z -direction may be found from summation of the standard deviation of each mode. In the calculations below only the first two eigenmodes are included, but the code may easily be expanded to include additional modes. The peak factor is found by time domain simulations.

2.5.1 Properties of the Turbulent Wind

Figure 2.3 shows that the girder is located between 26.08 and 37.87 meters above sea level. For simplicity reasons it has been chosen to look at the bridge as has a constant elevation height on 30 meters. The difference between the wind properties of a height on 20 and 40 meters above sea level are small [9] and as choosing larger height renders larger average mean velocity and lower turbulence intensity, and vice versa, the effect of increasing or decreasing the height within this interval only affects the results of the calculations minimally.

The critical wind direction is west-southwest, perpendicular to the bridge span. The wind is strongest from southwest, and values for this direction is used as this renders conservative results. Also, the difference between the values from southwest and west are small and the choice will have minor effect on the results. A report of the wind conditions in Dolmsundet performed by Norwegian Meteorological Institute on behalf of Norwegian Public Roads Administration states that 10 minutes mean wind velocity with a return period of 50 years at the height 30 meters above sea level is 38.4 m/s [9]. The same report concludes with an along wind turbulence component of $I_u = 0.14$ at 30 meters above sea level. The across wind turbulence component, I_w , is calculated from equation (1.25). The average length scales are calculated from equation (1.30) and (1.31) with $z_f = 30$ meters.

Other relevant wind parameters are presented in section 1.3.2 and 1.3.3. The necessary wind properties for the buffeting response calculations are summarized in table 2.2.

10 min. mean wind velocity, return period 50 yr	V	38.4 m/s
Air density	ρ	1.25 kg/m ³
Horizontal turbulence intensity	I_u	0.14
Vertical turbulence intensity	I_w	0.07
Average length scale of u-component	$x_f L_u$	139.04 m
Average length scale of w-component	$x_f L_w$	11.59 m
Kaimal parameter of u-component	$A_{u\omega}$	1.08
Kaimal parameter of w-component	$A_{w\omega}$	1.50
Co-spectrum parameter	c_{uy_f}	9
Co-spectrum parameter	c_{wy_f}	6

Table 2.2: Relevant buffeting wind properties

The nondimensional auto spectral density of the wind is shown in figure 2.5. It is calculated from the Kaimal spectrum as presented in equation (1.32). The figure shows that the wind mainly consists of low-frequency turbulence, especially the wind meeting the span perpendicularly, i.e. in u-direction. This indicates that lower eigenmodes of the bridge will represent the major part of the total response.

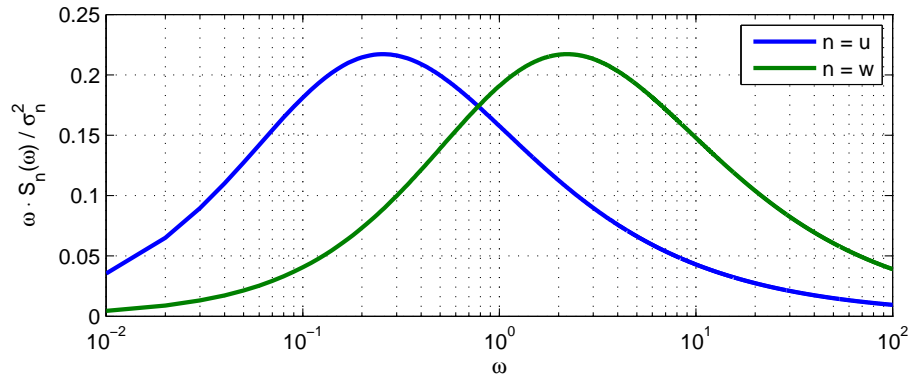
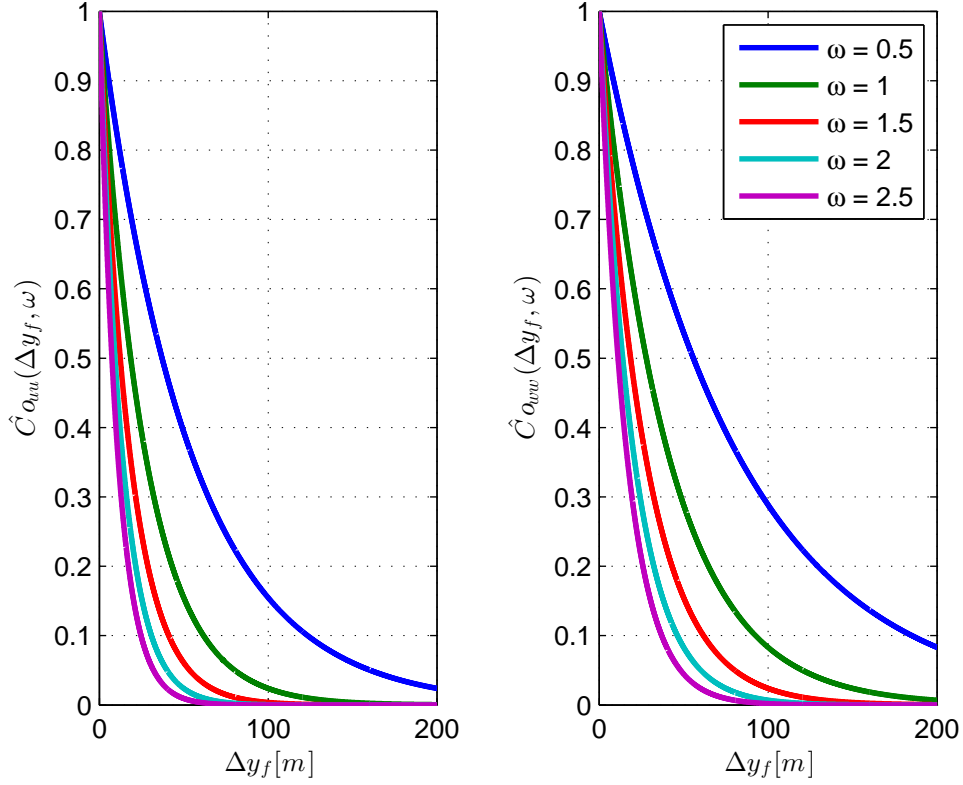


Figure 2.5: Nondimensional auto spectral density of the turbulent wind

It is assumed homogeneous wind conditions and equation (1.33) for the normalized co-spectrum of the wind field is adopted. Figure 2.6 shows how the normalized co-spectrum will vary with the across wind separation length Δy_f for different frequencies.

Figure 2.6: Normalized co-spectrum for selected values of ω

It should be observed that with this approximation of the co-spectrum the correlation for a separation length equal to the length of the cantilevered girders is practically zero for turbulence frequencies around the first two eigenfrequencies (1.401 and 1.687 rad/s). A consequence of this is that the action at the tip of the cantilevers on both sides will be as good as completely uncorrelated. The figure shows that the co-spectrum of the wind component in the along wind direction is descending faster with the separation length than the co-spectrum of the across wind component. The along wind turbulence is accordingly better correlated.

2.5.2 Load Coefficients

In order to determinate the load coefficients there has been performed wind tunnel tests on models of the cross section with different heights. The tests have shown that the lift coefficient is constantly $C_L = 0.51$, while the drag coefficient varies with the height [8]. The engineers at the Norwegian Public Roads Administration have divided the cross section into aero classes, see appendix A, where the cross sections in each class are

assigned a particular drag coefficient. They are presented in table 2.3. Aero class 10 is used for the elements with the casting unit. The drag coefficient for this aero class is scaled so that the original area of the element can be used in the calculations, hence the unreasonably high value.

Aero Class	Elements	Drag Coefficient
2	107-111 + 143-146	1.4
3	112-117 + 138-142	1.7
4	118-122 + 133-137	2.0
5	123-127 + 128-132	2.18
10	106 + 147	5.92

Table 2.3: Drag coefficients for the different cross sectional aero classes [8]

The derivatives of the drag- and lift coefficients are initially assumed to be zero. It seems reasonable that a rotation of the bridge beam does not affect the drag force in any large extent. $C'_D = 0$ was also used in the calculations of dynamic response of Raftsundet Bridge, a similar balanced cantilever bridge, where the calculated response showed good compliance with the measured response [10]. The lift force could on the other hand be affected by rotation of the girder, especially for rotation of the parts of the girder with large cross sectional height. This is supported by E. Strømmen, E. Hjort-Hansen and J. H. Kaspersen [11]. C'_L is therefore included in the equations, but is zero until it is further discussed in section 3.3.

The moment coefficients are irrelevant because of the characteristic high torsional stiffness of a box girder.

2.5.3 Frequency Response

The aerodynamic coefficients are introduced in section 1.5.1. Because $K_{ae_y} = K_{ae_z} = 0$, as shown in equation (1.48), κ_{ae_y} and κ_{ae_z} must be zero for all eigenmodes. Inserting for $\tilde{C}_{ae_i} = \int_{L_{exp}} \phi_i^2 \cdot C_{ae_i} dx$ in the expression of ζ_{ae_i} , where C_{ae_i} is given in equation (1.47), $i = y$ or z , and assuming that the entire span is exposed to wind, i.e. $L_{exp} = L$, the damping coefficients for $V = 38.4$ m/s will be

$$\zeta_{ae_1} = \frac{\tilde{C}_{ae_y}}{2\omega_1 \tilde{M}_1} = -\frac{\rho V}{2\omega_1 \tilde{m}_1} \cdot \frac{\int_L \phi_{1,y}^2 \cdot D(x) \cdot \bar{C}_D(x) dx}{\int_L \phi_{1,y}^2 dx} = -0.0093 \quad (2.2)$$

$$\zeta_{ae_2} = \frac{\tilde{C}_{ae_z}}{2\omega_2 \tilde{M}_2} = -\frac{\rho V}{4\omega_2 \tilde{m}_2} \cdot \frac{\int_L \phi_{2,z}^2 (B \cdot C'_L(x) + D(x) \cdot \bar{C}_D(x)) dx}{\int_L (\phi_{2,z}^2 + \phi_{2,x}^2) dx} = -0.0068 \quad (2.3)$$

The aerodynamic damping coefficients are used to find the frequency response of the bridge by equation (1.62). Figure 2.7 shows the frequency response for the first two eigenmodes. The second mode has a slightly higher frequency response peak due to the lower absolute value of the aerodynamic damping coefficient, indicating that this mode is more vulnerable against resonant frequencies. The first mode has its peak for a lower frequency and the response of this mode will presumably be larger because the wind mainly consists of low-frequency turbulence, cf. figure 2.5.

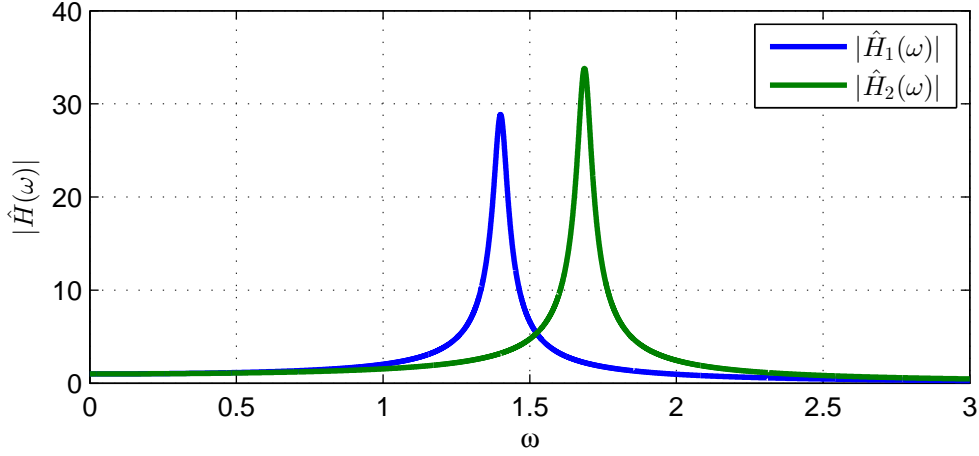


Figure 2.7: Frequency response of mode 1 and 2

2.5.4 Buffeting Load Spectrum

The derivation of the buffeting load spectrum and joint acceptance function in section 1.5.3 is made on the presumption that the cross sectional dimensions are constant. This is nearly never the case for balanced cantilevered bridges as they need considerably higher moment capacity close to the pillar than at the midspan. In the case of Dolmsundet bridge the cross sectional height, the drag coefficient and probably also the derivative of the lift coefficient will vary along the span, while the width and the lift coefficient are constant. The derivative of the drag coefficient is assumed negligible resulting in the following expressions of the joint acceptance functions for the first two eigenmodes

$$J_1^2(\omega) = \iint_L \phi_{1,y}(x_1) \cdot \phi_{1,y}(x_2) \left\{ \left[\left(\frac{2 \cdot I_u}{B} \right)^2 D(x_1) \cdot \bar{C}_D(x_1) \cdot D(x_2) \cdot \bar{C}_D(x_2) \right] \right. \\ \left. \hat{C}_{ouu}(\Delta x, \omega) \cdot \frac{S_u(\omega)}{\sigma_u^2} + [\bar{C}_L I_w]^2 \cdot \hat{C}_{oww}(\Delta x, \omega) \cdot \frac{S_w(\omega)}{\sigma_w^2} \right\} dx_1 dx_2 \quad (2.4)$$

$$J_2^2(\omega) = \iint_L \phi_{2,z}(x_1) \cdot \phi_{2,z}(x_2) \cdot \left\{ \left[2\bar{C}_L I_u \right]^2 \hat{C}_{o_{uu}}(\Delta x, \omega) \cdot \frac{S_u(\omega)}{\sigma_u^2} + \left[\left(C'_L(x_1) + \frac{D(x_1) \cdot \bar{C}_D(x_1)}{B} \right) \cdot \left(C'_L(x_2) + \frac{D(x_2) \cdot \bar{C}_D(x_2)}{B} \right) \cdot I_w^2 \right] \hat{C}_{o_{ww}}(\Delta x, \omega) \cdot \frac{S_w(\omega)}{\sigma_w^2} \right\} dx_1 dx_2 \quad (2.5)$$

The buffeting modal load spectra are calculated by

$$S_{\tilde{Q}_i}(\omega) = \left[\frac{\rho V^2 B}{2} J_i(\omega) \right]^2 \quad \text{where } i = 1, 2 \quad (2.6)$$

Figure 2.8 shows a plot of the buffeting modal load spectra for mode 1 and 2. It should be observed that there are practically no loads with frequencies higher than 1.4 rad/s, which corresponds to the lowest eigenfrequency. This indicates that the background part will dominate the response.

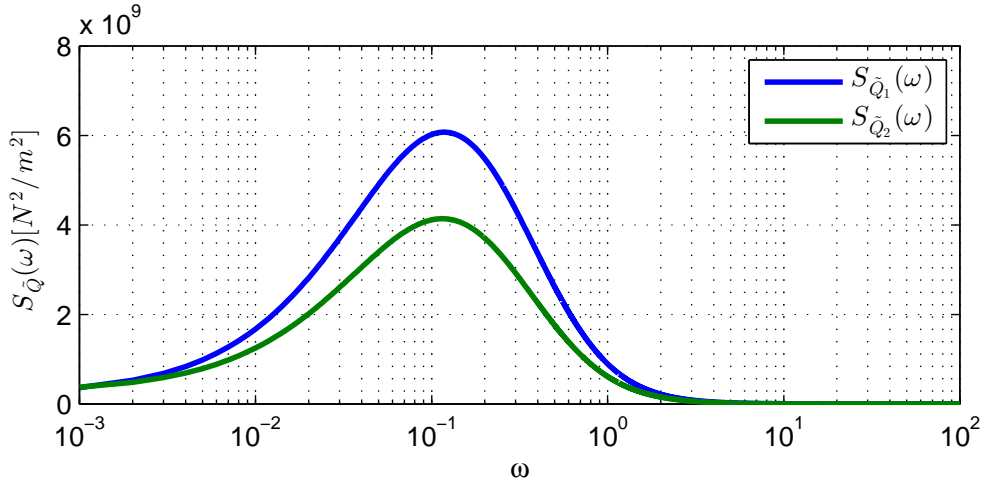


Figure 2.8: Buffeting modal load spectrum

2.5.5 Buffeting Response

The first mode describes displacement purely in y -direction, while the second mode describes displacement in both z - and x -direction. Wind on the pillar is as mentioned neglected so that the standard deviation of the response of mode 1 and 2 may be found from equation 1.71 and 1.73 respectively. The standard deviation of the response in y - and z -direction when including the first two eigenmodes are by this

$$\sigma_{r_y}(x_r) = \sigma_{r_{1,y}}(x_r) = |\phi_{1,y}(x_r)| \cdot \frac{\rho V^2 B}{2\tilde{m}_1 \omega_1^2} \cdot \left[\int_0^\infty |\hat{H}_1(\omega)|^2 \cdot \hat{J}_1^2(\omega) d\omega \right]^{1/2} \quad (2.7)$$

$$\sigma_{r_z}(x_r) = \sigma_{r_{2,z}}(x_r) = |\phi_{2,z}(x_r)| \cdot \frac{\rho V^2 B}{2\tilde{m}_2 \omega_2^2} \cdot \left[\int_0^\infty |\hat{H}_2(\omega)|^2 \cdot \hat{J}_2^2(\omega) d\omega \right]^{1/2} \quad (2.8)$$

where the normalized joint acceptance functions are given as

$$\hat{J}_1^2(\omega) = \frac{J_1^2(\omega)}{\left(\int_L \phi_{1,y}^2 dx \right)^2} \quad (2.9)$$

$$\hat{J}_2^2(\omega) = \frac{J_2^2(\omega)}{\left(\int_L (\phi_{2,z}^2 + \phi_{2,x}^2) dx \right)^2} \quad (2.10)$$

The standard deviations of the response of the cantilevered girders are plotted in figure 2.9. The highest response will naturally occur at the tip of the longest cantilever, see figure 2.3. The maximum values are: $\sigma_{r_y}(x = -98.7) = 0.139$ m and $\sigma_{r_z}(x = -98.7) = 0.076$ m.

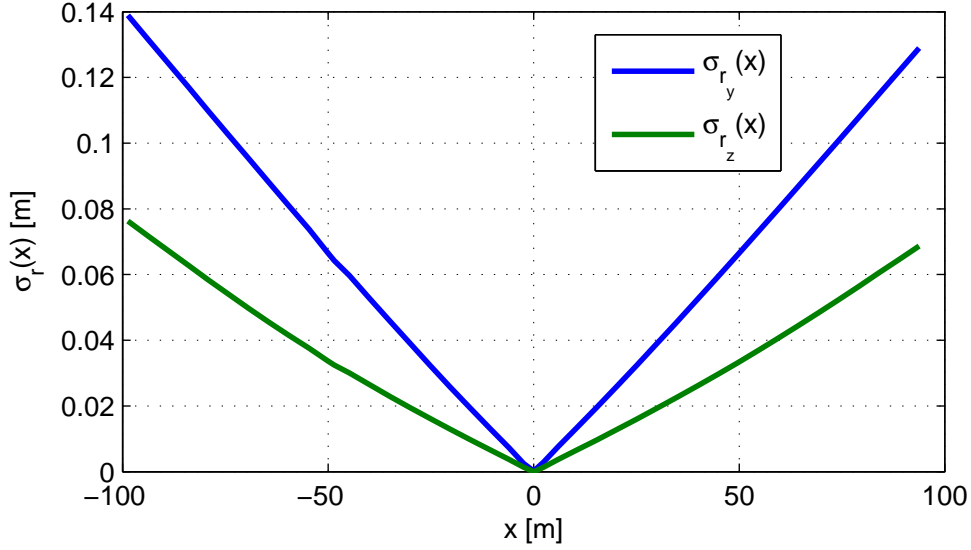


Figure 2.9: Standard deviation of the displacement in y - and z -direction

The peak factors are found by time domain simulations, using equation (1.119). One simulation is shown in figure 2.10.

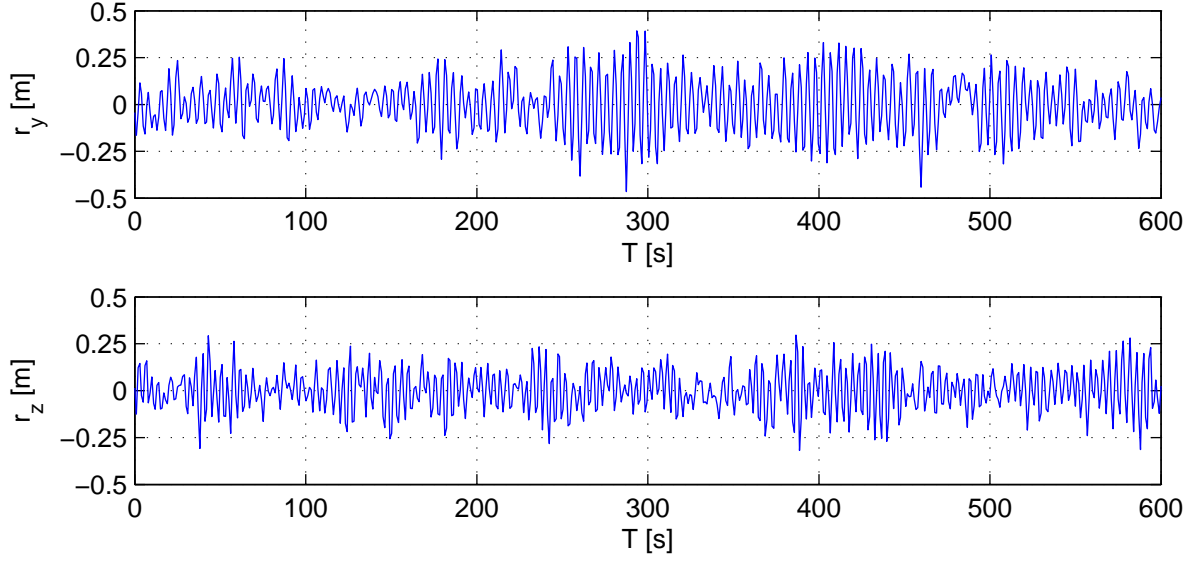


Figure 2.10: Time domain simulation of the response

The simulations are performed 10 times, and the peak factors from each simulation and the mean values are presented in table 2.4.

Nr.	1	2	3	4	5	6	7	8	9	10	Mean
k_{p_y}	3.203	3.401	3.559	3.860	3.121	3.237	2.693	2.893	2.875	2.907	3.175
k_{p_z}	3.163	3.211	2.698	3.299	3.062	2.926	3.564	2.609	2.805	3.226	3.056

Table 2.4: Peak factors from time domain simulations

This renders a maximum displacement in respectively y - and z -direction on

$$r_{y_{max}}(x_r = -98.7) = k_{p_y} \cdot \sigma_{r_y}(x_r = -98.7) \approx 0.44 \text{ m} \quad (2.11)$$

$$r_{z_{max}}(x_r = -98.7) = k_{p_z} \cdot \sigma_{r_z}(x_r = -98.7) \approx 0.23 \text{ m} \quad (2.12)$$

2.6 Vortex Shedding Calculations

This section includes the calculation of the vortex shedding induced dynamic response of Dolmsundet Bridge in the critical construction stage. The vortex shedding phenomenon induces primarily loads in z - and θ -direction, as described in section 1.4.2. In the case of Dolmsundet Bridge the torsional stiffness of the girder is large and consequently will the eigenmodes corresponding to rotation of the girder have high eigenfrequencies such that loads in θ -direction only creates negligible forces. Also, the main concern at the

construction stage is the capacity of the pillar, which is virtually unaffected by the rotation of the bridge beam. Therefore only the response of vortex shedding in the vertical direction, i.e. due to mode 2, is evaluated.

As for the buffeting calculations the mean displacement is zero, because this situation will induce the largest moment in the pillar. Thus is the maximum displacement

$$r_{max}(x_r) = k_p \cdot \sigma_r(x_r) \quad (2.13)$$

The standard deviation will be found by solving the second degree equation presented in the theory part, and the peak factor will be found by time domain simulations.

2.6.1 Simplified Model

The derivation of the standard deviation of vortex shedding induced response which is presented in previous parts of this report is based on the presumption that the cross sectional dimensions are constant. There are in general few publications about vortex shedding induced response of bridges with varying cross sectional dimensions. It is therefore chosen to simplify the system representing Dolmsundet Bridge in the critical construction stage into a balanced cantilever bridge with constant girder height. It is assumed that only approximately half of the cantilevers will be influenced by vortex shedding as the cross section of the half closest to the pillar is considerably higher, see appendix A. This will introduce some inaccuracy in the result, but it is considered as the best option as more detailed calculations will demand extensive research.

Element 106 to 117 and element 138 to 147 is assumed exposed to the vortex shedding induced loads. See appendix A for the element division. The average height when looking at only this part of the girder is $D \approx 3.4$ m. Figure 2.11 shows the simplified model of the bridge in the critical construction stage.

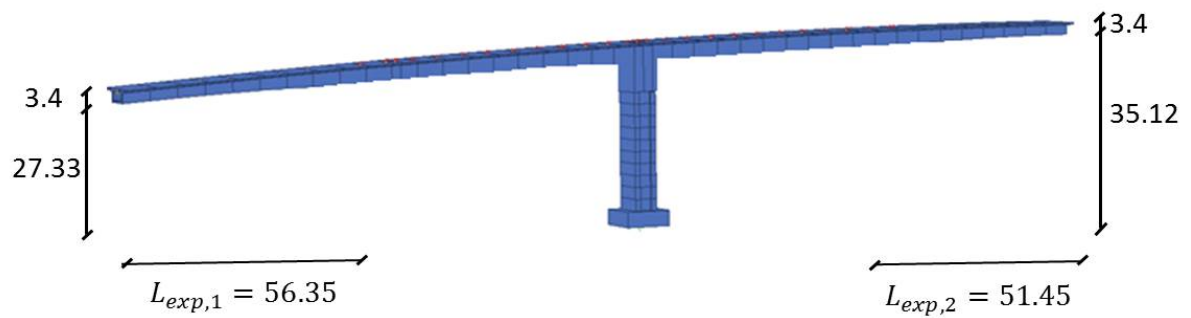


Figure 2.11: Simplified model of Dolmsundet Bridge in the critical construction stage

2.6.2 Properties of the Vortex Shedding Induced Wind Loads

It has not been performed vortex shedding experiments directed against this particular case, properties of the vortex shedding induced wind loads must therefore be based on previous experience. Eurocode 1 states that a rectangular cross section with the relationship $B/D \approx 3.3$ has a Strouhal number on approximately 0.11 [12]. The nondimensional load spectrum band width parameter b_z has typically a value between 0.1 and 0.3, and the nondimensional coherence length λ_z between 2 and 5 [1, page 106]. After consultation with Einar N. Strømmen [13] the remaining relevant parameters are chosen. The parameters are summed up in table 2.5.

Air density	ρ	1.25 kg/m ³
Strouhal number	St	0.11
Nondimensional root mean square lift coefficient	$\hat{\sigma}_{q_z}$	1
Nondimensional load spectrum band width parameter	b_z	0.15
Parameter for the self-limiting characteristic	a_z	0.4
Nondimensional coherence length scale	λ	2
Reference value for velocity dependent damping coefficient	$K_{a_z, max}$	0.2

Table 2.5: Relevant wind properties for vortex shedding induced response

Equation (1.49) is used to find the mean wind velocity corresponding to the largest response of the second eigenmode

$$V_R = \frac{\omega}{2\pi} \cdot \frac{D}{St} = \frac{1.687}{2\pi} \cdot \frac{3.4}{0.11} \text{ m/s} \approx 8.3 \text{ m/s} \quad (2.14)$$

As expected the vortex shedding induced response will reach its peak for a relatively low mean wind velocity. This supports the choice of calculating buffeting and vortex shedding induced response separately, as the buffeting response in z -direction will be low for this low wind velocity.

2.6.3 Aerodynamic Damping

The aerodynamic damping coefficient may be calculated from equation (1.83), with $C_{ae_i} = C_{ae_z}$ from equation (1.53), rendering

$$\zeta_{ae_2} = \frac{\tilde{C}_{ae_2}}{2\omega_2 \tilde{M}_2} = \frac{\rho B^2}{4\tilde{m}_2} \cdot K_{a_z} \cdot \left[1 - \left(\frac{\sigma_{r_z}}{a_z D} \right)^2 \right] \cdot \frac{\int_{L_{exp}} \phi_2^2 dx}{\int_L \phi_2^2 dx} \quad (2.15)$$

It is chosen to use $K_{a_z, max}$ for K_{a_z} , which is consistent with an assumption of smooth air flow. This is a seldom phenomenon, but using $K_{a_z, max}$ will render conservative results and there is no information to base a possible velocity dependent expression on.

Figure 2.12 shows how the aerodynamic damping coefficient will vary with the response. The factor a_z takes care of the self-limiting characteristic of vortex shedding induced response described in section 1.4.2. For values of σ_{r_z} larger than $a_z D$ the aerodynamic damping is insignificant.

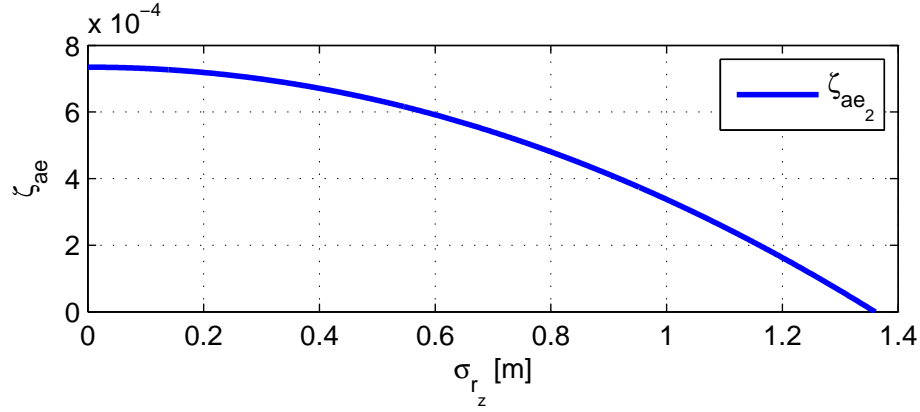


Figure 2.12: The aerodynamic damping coefficient of mode 2 plotted against σ_{r_z}

The structural damping coefficient is 0.008, considerably larger than the aerodynamic damping coefficient, indicating that the latter will have less influence on the response.

2.6.4 Vortex Shedding Load Spectrum

The normalized vortex shedding co-spectrum is calculated by equation (1.51). Figure 2.13 shows the co-spectrum plotted against the along span separation length Δx .

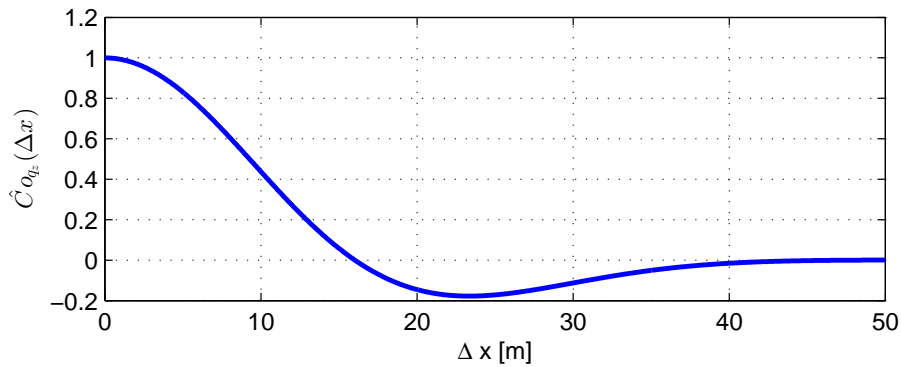


Figure 2.13: The normalized vortex shedding co-spectrum in z-direction

It is observed that the wind point load at two points with a separation length larger than 41 meters are entirely uncorrelated, and that the co-spectrum is negative for separation lengths between 16 and 41 meters.

The integral length scale of the vortices are calculated and may as expected be approximated by $\lambda_z D = 6.8$ m

$$\int_0^\infty \hat{C}o_{q_z}(\Delta x) d(\Delta x) = 6.7\text{m} \quad (2.16)$$

As seen the integral length scale of the vortices is considerably smaller than the length of the cantilevered girders so that the load spectrum may be calculated by equation (1.80). Inserting the single point load spectrum from equation (1.50) into equation (1.80) renders the following expression of the modal load spectrum

$$S_{\hat{Q}_2}(\omega) = 2\lambda D \cdot \frac{\left(\frac{1}{2}\rho V^2 \cdot B \cdot \hat{\sigma}_{q_z}\right)^2}{\sqrt{\pi} \cdot \omega_s \cdot b_z} \cdot \exp\left\{-\left(\frac{1 - \omega/\omega_s}{b_z}\right)^2\right\} \cdot \int_{L_{exp}} \phi_2^2(x) dx \quad (2.17)$$

The modal load spectrum for the resonant mean wind velocity, i.e. the mean wind velocity that renders $\omega_s = \omega_2$, is shown in figure 2.14.

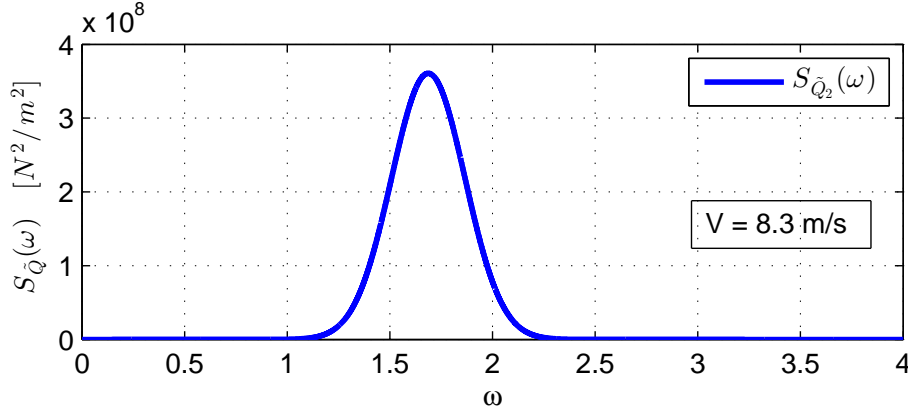


Figure 2.14: Vortex shedding modal load spectrum

2.6.5 Vortex Shedding Response

The standard deviation of the response due to vortex shedding may be found by equation (1.91) with $\hat{\zeta}_m$ and $\hat{\beta}_m$ from equation (1.93) and (1.94). The maximum standard deviation will occur when $V = V_R$, i.e. when the vortex shedding frequency is similar to the eigenfrequency. Figure 2.15 shows the standard deviation of the response plotted against the mean wind velocity and along the girder. The maximum value is $\sigma_{r_z}(x_r = -98.7) = 0.130$ m.

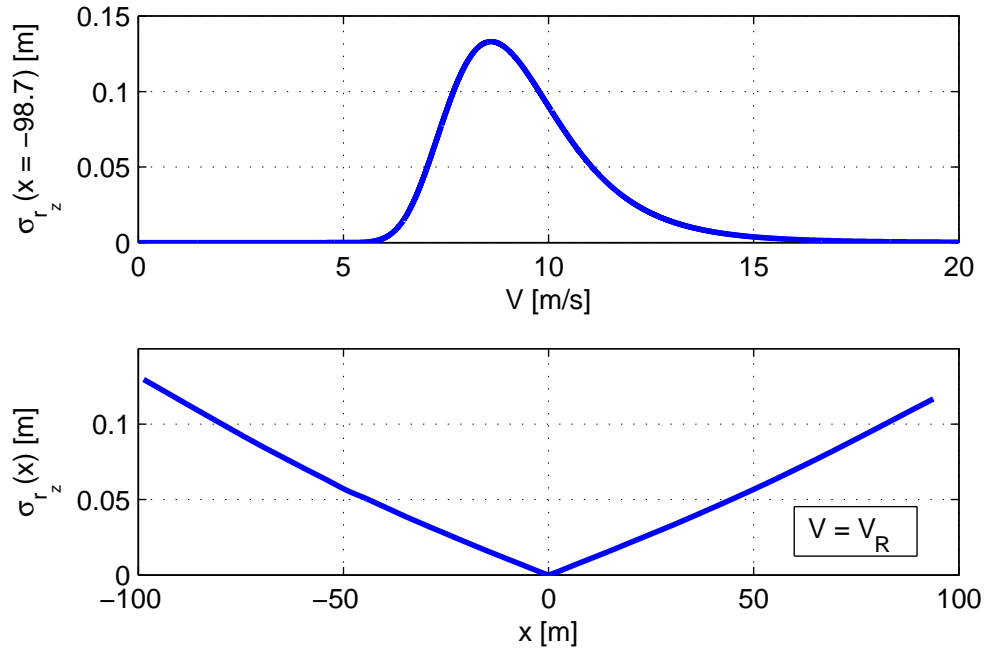


Figure 2.15: Top: standard deviation of the response at the tip of the longest cantilever, bottom: standard deviation of the response along the girder at resonance

The peak factor is found by time domain simulations, using equation (1.119). One simulation is shown in figure 2.16.

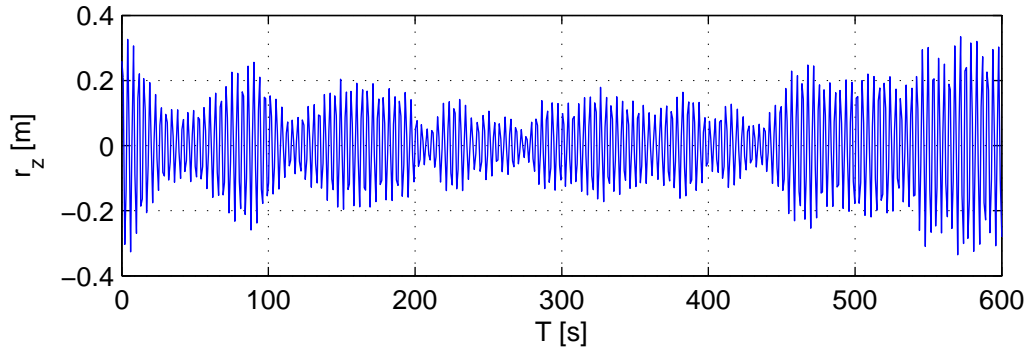


Figure 2.16: Time domain simulation of the response

The simulation is as for buffeting response performed 10 times. The result is presented in table 2.6.

Nr.	1	2	3	4	5	6	7	8	9	10	Mean
k_{p_z}	3.362	3.087	3.373	2.303	2.736	2.434	2.272	1.998	2.192	2.531	2.63

Table 2.6: Peak factors from time domain simulation

Thus is the maximum displacement

$$r_{z_{max}}(x_r = -98.7) = k_{p_z} \cdot \sigma_{r_z}(x_r = -98.7) \approx 0.34 \text{ m} \quad (2.18)$$

It is seen that the vortex shedding induced response is larger than the buffeting induced response of mode 2.

2.7 Maximum Displacements

It is as mentioned the cross sectional forces in the pillar that is the main concern regarding wind induced loads. This section describes the maximum wind induced displacements of the bridge in the construction stage, which may be used for further design of the bridge. The calculations of forces when displacements are known are considered trivial and will not be included in the report.

The two cases for consideration are the buffeting induced response of the first mode exposed to the 10 minute mean wind velocity with return period of 50 years, presented in figure 2.17, and the resonant vortex shedding induced response of the second mode, presented in figure 2.18.

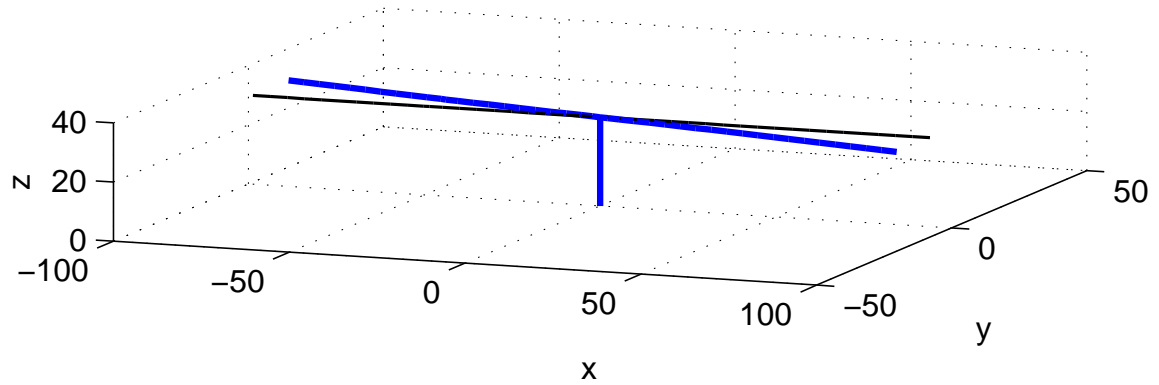


Figure 2.17: Mode 1 (for illustrative purpose multiplied by 30)

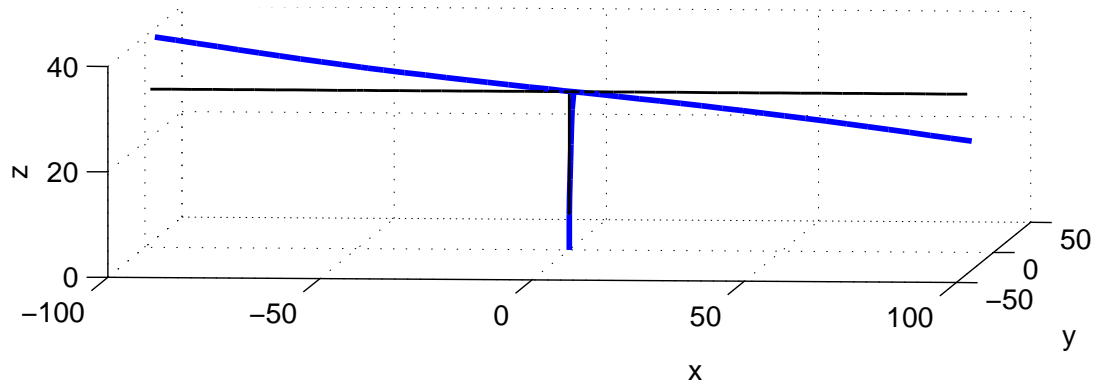


Figure 2.18: Mode 2 (for illustrative purpose multiplied by 30)

For the calculations of the rotation of the top of the pillar the mode shapes are approximated linear functions. Figure 2.19 shows the eigenmodes plotted with linear functions. It is seen that within the interval $-20 \geq x \leq 20$ the linear approximation is appropriate.

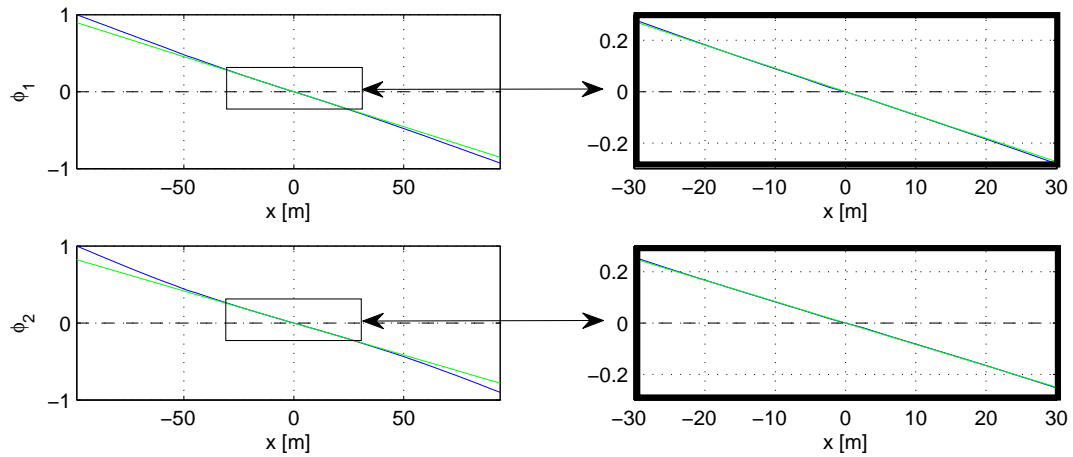


Figure 2.19: Linear approximation of the eigenmodes

Relevant maximum displacements and rotations are presented in table 2.7. They may be used directly to estimate the cross sectional forces.

Mode 1	Mode 2
$r_y(x_r = -98.7) = 0.44 \text{ m}$	$r_z(x_r = -98.7) = 0.34 \text{ m}$
$r_y(x_r = 93.8) = -0.41 \text{ m}$	$r_z(x_r = 93.8) = -0.31 \text{ m}$
$r_{\theta_z}(x_r = 0) = 0.0040 \text{ rad}$	$r_{\theta_y}(x_r = 0) = 0.0029 \text{ rad}$
	$r_x(x_r = 0) = 0.04 \text{ m}$

Table 2.7: Maximum wind induced displacements and rotations

3 Sources of Errors

The calculations performed above include many simplifications and assumptions which may induce inaccuracy. The damping properties are difficult to predict and is often highlighted as an element of uncertainty, but there are also other sources of errors that need to be considered. For instance the assumption of the derivative of the lift coefficient as zero, the different vortex shedding properties and the function adopted for the buffeting co-spectrum. Some of the possible sources of errors and the results' sensitivity towards them are discussed below.

3.1 Wind on Pillar

Wind on the pillar is neglected; this may create some inaccuracy for the response in z-direction. But it is likely that the effect on the response from wind on the pillar is small compared to the vortex shedding induced response, this is supported by two publications by respectively K. Aas-Jakobsen Jr., K. Aas-Jakobsen, E. Strømmen [10] and E. Strømmen, E. Hjort-Hansen, J. H. Kaspersen [11]. Both publications have found a good correlation between the response found from experiments and from calculations by the vortex shedding theory where wind on the pillar is neglected.

3.2 Elevation Height

It is used the same elevation height on 30 meters above sea level for the entire girder when performing the buffeting response calculations, see section 2.5.1. This means that the mean wind velocity, the turbulence intensity and the average length scale of the turbulence are somewhat inaccurate. Table 3.2 shows values of these variables for different elevation levels.

Elevation level	z_f	25 m	30 m	35 m	40 m
Mean wind velocity [9]	V [m/s]	37.4	38.4	39.1	39.8
Horizontal turbulence intensity [9]	I_u [-]	0.145	0.140	0.135	0.130
Vertical turbulence intensity, eq. (1.25)	I_w [-]	0.073	0.070	0.068	0.065
Average length scale of u-comp., eq. (1.30)	$^{x_f}L_u$ [m]	131.64	139.04	145.62	151.57
Average length scale of w-comp., eq. (1.31)	$^{x_f}L_w$ [m]	10.97	11.59	12.13	12.63

Table 3.1: Variation of the properties depending on the elevation level

The table shows that variations are small, and while the turbulence intensity decreases with the height the mean wind velocity increases, so that they to some extent compensate for each other. Figure 3.1 shows the buffeting response for different choices of a constant elevation level. It is observed that the choice of the elevation level within this interval has minimal effect on the result.

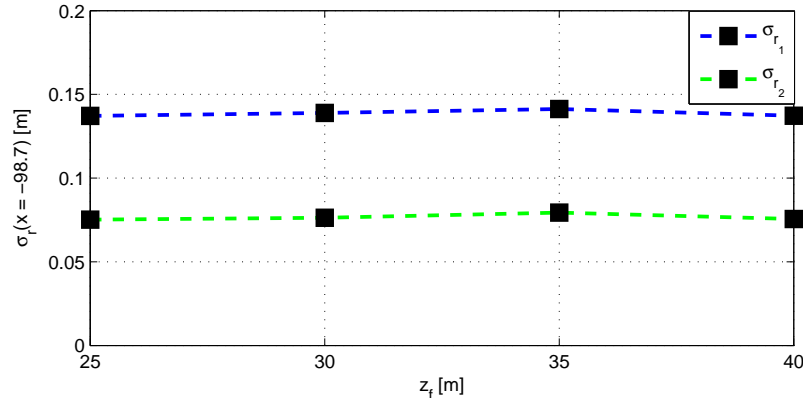


Figure 3.1: The effect of using a different constant elevation height

3.3 Load Coefficients

The drag and lift coefficients are received from the Norwegian Public Roads Administration, and are assumed to represent no source of error. The derivative of the load coefficients with respect to the angle of incidence is initially assumed zero, but experiments on similar cross sections have shown that C'_L might obtain a negative value between 0 and -2.8 [10] [11]. Figure 3.2 shows the results from wind tunnel tests on models of a rectangular box girder with width on 10.2 meters and heights on 4, 8 and 12 meters. It is uncertainty around whether the results may be directly applied to the calculations of Dolmsundet Bridge, as the protruding flanges represent close to 1/3 of the width of the cross section of Dolmsundet Bridge and only 1/8 of the width of the model cross section. The results are nevertheless presented here to show a possible instability phenomenon.

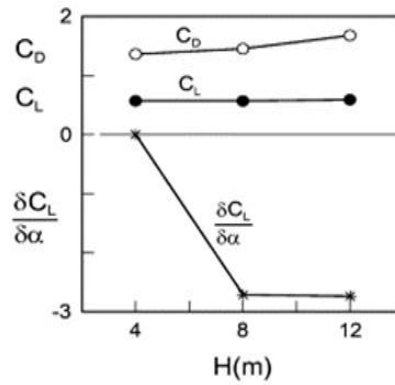


Figure 3.2: Load coefficients for example model [11]

Figure 3.2 shows that the derivative of the lift coefficient is negative and consequently will reduce the total damping, i.e. increase the aerodynamic damping coefficient, see

equation (2.3). The motion induced instability named galloping will occur if $\zeta = \zeta_{ae}$ [1, page 200]. Figure 3.3 shows the response of mode 2 for different values of C'_L when C'_L is assumed constant, i.e. independent of the height of the cross section. This is presumably not the case, but the value at the tip of the cantilevers will give the largest contribution to the response because $D(x) \cdot \bar{C}_D(x)/B$ is low and $\phi_2(x)$ is high here, see equation (2.5). Assuming a constant C'_L will therefore give a good indication of the critical value of C'_L for the parts of the girder furthest from the pillar.

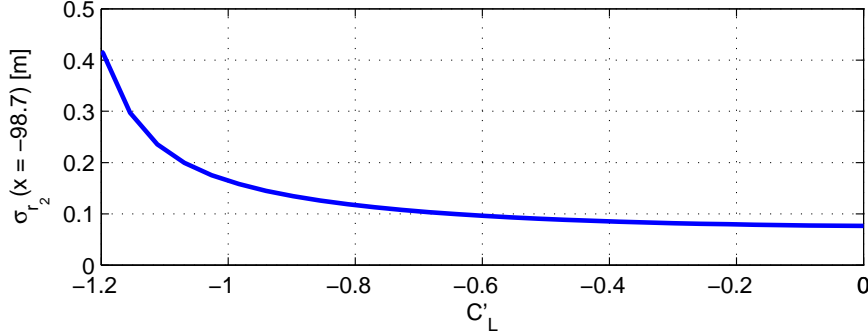


Figure 3.3: Buffeting response of mode 2 plotted against constant C'_L

It is seen that in order to avoid instability it is important that C'_L for cross sections far from the pillar does not obtain large negative values.

3.4 Motion Induced Effects

For the calculations above it was assumed that the wind velocity was well below any instability limit, and that motion induced effects could be neglected. The section above describes that instability due to galloping might be an issue, and should be further investigated.

Also, the aerodynamic damping coefficients due to buffeting wind have relatively large absolute values, $|\zeta_{ae1}| = 0.0093$ and $|\zeta_{ae2}| = 0.0068$, see equation (2.2) and (2.3), while the proposed structural damping coefficient from the Norwegian Public Roads Administration is 0.008 for all modes [7]. Thus, the effect of the aerodynamic damping is considerable and the assumption of $\omega(V) = \omega(V = 0)$ may not be consistent with the actual response of the bridge. At the same time the calculated response is relatively small, indicating that the motion induced effects are small.

The calculated aerodynamic damping coefficient for vortex shedding is in the region of $0 \geq \zeta_{ae2} \geq 0.00074$, see figure 2.12, much smaller than the structural damping coefficient, so it seems reasonable to neglect motion induced effects in the vortex shedding calculations.

3.5 Buffeting Co-Spectrum

The buffeting wind's normalized co-spectrum is assumed an exponential function on the form

$$\hat{C}o_{nn}(\Delta y_f, \omega) = \exp\left(-c_{ny_f} \cdot \frac{\omega \cdot \Delta y_f}{2\pi \cdot V(z_f)}\right) \quad n = u, v, w \quad (3.1)$$

The function approaches 1 for $\omega \rightarrow 0$ for all values of Δs , which is obviously not correct. Nor does it consider the possibility of negative correlation, a possibility that should be paid attention to when eigenmodes have both positive and negative values. In addition the chosen values of c_{ny_f} are only a first approximation, and as this parameter considerably alters the calculated response it is recommended to perform investigation towards finding values fitted to the particular case. Figure 3.4 shows that the buffeting induced response in the along wind direction is highly dependent on the choice of c_{uy_f} and to some extent c_{wy_f} . It should be observed that by decreasing the correlation with higher values of c_{uy_f} or c_{wy_f} the response will decrease. The same is observed for buffeting induced response in the across wind direction.

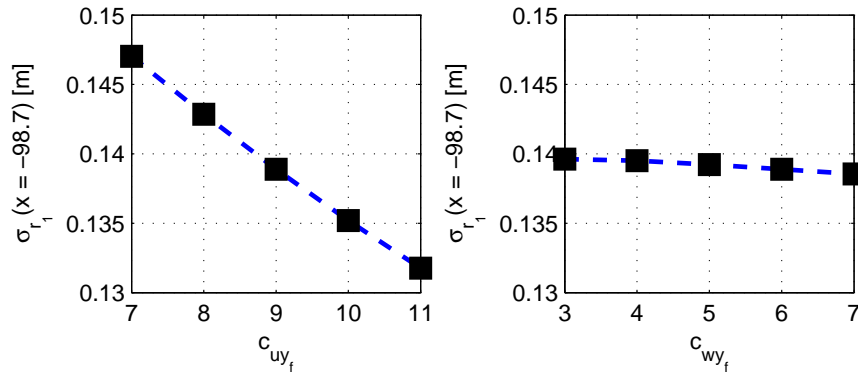


Figure 3.4: Buffeting induced response in the along wind direction for different values of the correlation parameters

3.6 Vortex Shedding Parameters

To be able to use the theory behind vortex shedding response calculations the cross section was assumed to have a constant cross sectional height, see figure 2.11, and it was assumed that only approximately half of the girder was simultaneously exposed to vortex shedding induced loads. Appendix A and B show that the half of the girder closest to the pillar has considerably higher cross section, and it is therefore reasonable to assume that this part will not be excited by the same frequency as the part of the girder with

lower cross sectional height. The choice of the size L_{exp} will not be of great importance as it is the action furthest from the pillar that will have the largest effect on the pillar's stress resultants. The assumed constant height, D , will possibly affect the calculations and should be carefully chosen.

In addition it is not performed any tests on the particular bridge regarding the vortex shedding properties so the chosen values presented in table 2.5 are uncertain. Especially the nondimensional root mean square lift coefficient, $\hat{\sigma}_{q_z}$, and the velocity dependent damping coefficient, K_{a_z} , are difficult to predict [13]. Figure 3.5 shows the effect of varying these variables. It is seen that $\hat{\sigma}_{q_z}$ greatly affects the response, and should be chosen with care. K_{a_z} is velocity dependent [1, page 107], but is in the calculations above assumed constant as there is no information to base a possible expression on and a constant value renders conservative results. It is seen from figure 3.5 that the choice of this constant affects the results minimally. This is because the aerodynamic damping coefficient regardless will be small compared to the structural damping coefficient.

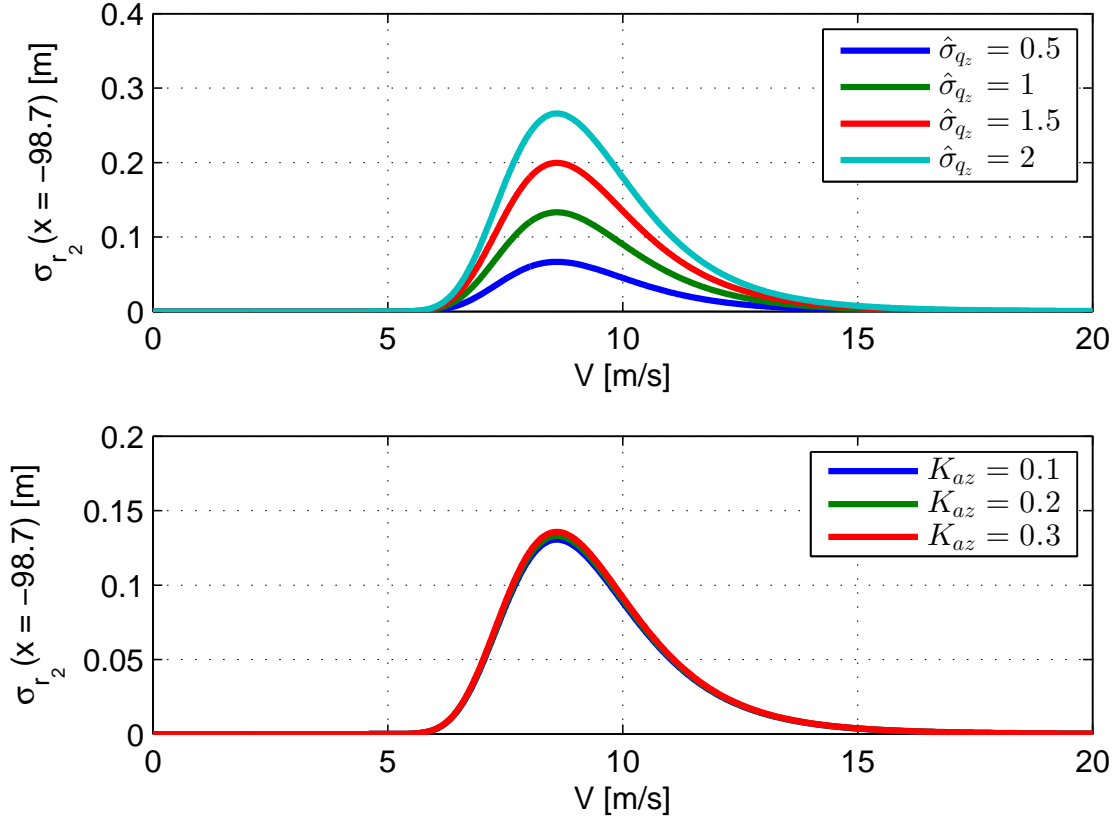


Figure 3.5: The sensitivity of vortex shedding response towards chosen variables

3.7 Structural Damping

As mentioned the structural damping coefficient is an element of uncertainty in structural dynamic calculations. Figure 3.6 shows how the damping coefficient will alter the response. Naturally the alteration is largest for the modes with the lowest aerodynamic damping coefficients. Vortex shedding response will as expected be very large if the structural damping is small, but the self-limiting effect will occur at standard deviations at approximately $\sigma_{r_z} = a_z D = 1.36$ m. It is observed that even if the structural damping should be considerably lower than assumed, the response will not be substantially altered.

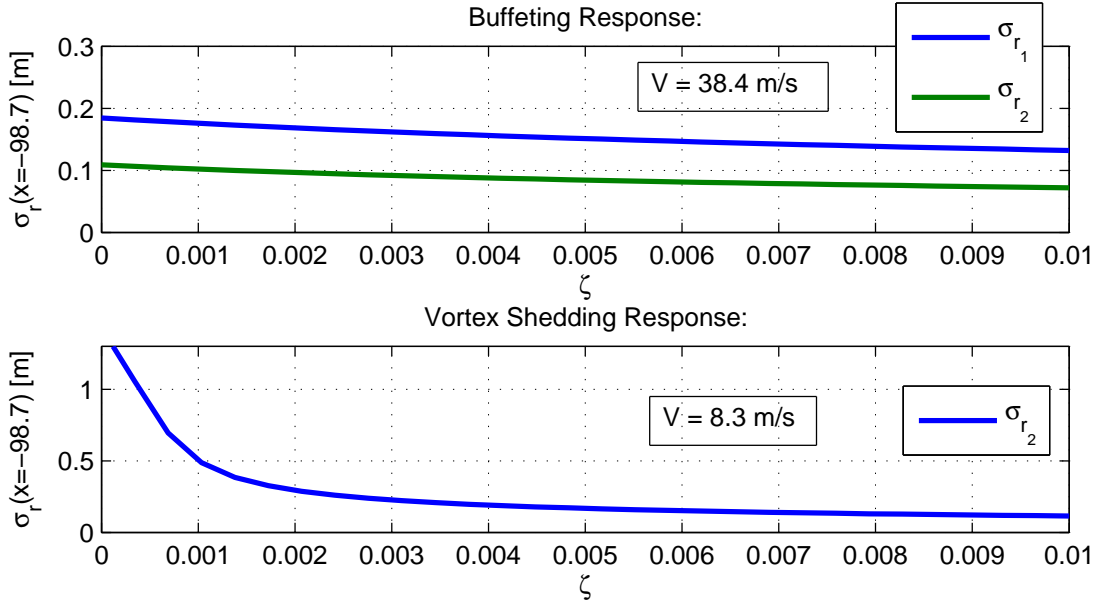


Figure 3.6: Response plotted against structural damping

3.8 Numerical Integration

The calculations are performed by numerical computations in MATLAB. For all integrations except the calculation of the joint acceptance the values received from the Norwegian Public Roads Administration are used directly, such that the step size equals to the element size, see appendix A and B. The joint acceptance function includes the co-spectrum function which is an exponential function of Δx , demanding a smaller step size to avoid numerical integration errors. This is achieved by prolonging the vectors $\phi(x)$, $D(x)$ and $\bar{C}_D(x)$ by interpolation, and divide the elements into smaller lengths. The variable *div* is the number of divisions of each of the elements, whereas the largest elements are 4.9 meters.

The step size when integrating over ω must also be small enough to avoid error in the numerical integration. Table 3.2 shows the buffeting response and the error for different choices of integration step sizes. The response for the 0.001 frequency step and $div = 20$ is set as the basis of the error.

Frequency step size	Division of each element	$r_{y,max}$	error	$r_{z,max}$	error
0.1	1	0.1658	19.5 %	0.0759	0.4 %
0.1	4	0.1652	19.0 %	0.0755	0.9 %
0.1	20	0.1651	18.9 %	0.0755	0.9 %
0.01	1	0.1394	0.4 %	0.0767	0.7 %
0.01	4	0.1389	0.1 %	0.0763	0.1 %
0.01	20	0.1388	0 %	0.0762	0 %
0.001	1	0.1394	0.4 %	0.0767	0.7 %
0.001	4	0.1389	0.1 %	0.0763	0.1 %
0.001	20	0.1388	0 %	0.0762	0 %

Table 3.2: Numerical error

It is seen that a frequency step size of 0.01 and a division of each element into 4 give an error on 0.1 %, which is considered accurate enough. The response, especially response in z-direction, is relatively independent of the integration step size, this indicates that the response consists mainly of a background part.

4 Conclusion

This thesis contains a theoretical study of wind induced dynamic response of line-like structures, followed up by calculations of the response of Dolmsundet Bridge in the critical construction stage and a discussion of possible sources of error.

The buffeting and vortex shedding induced response have been calculated using the procedures presented in the theoretical study. A computational program was made in MATLAB. The standard deviations were found by a frequency domain approach while the peak factors were found from time domain simulations. No static calculations were included in the report. It was assumed that the major part of the response was related to the first two eigenmodes, the first in the along wind direction, and the second in the vertical direction. It was assumed uncoupled, single component modes, no motion induced effects, and homogeneous and Gaussian distributed wind velocity.

The buffeting wind properties were taken from a report on the wind conditions in the specific area. A return period on 50 years was used.

The calculations showed that vortex shedding induced response would be larger than buffeting induced response of the mode in z -direction. The figures below show the calculated response of the bridge for the first two eigenmodes. The tip displacements of the longest cantilever were found to be $r_y = 0.44$ m for mode 1 , and $r_z = 0.34$ m for mode 2.

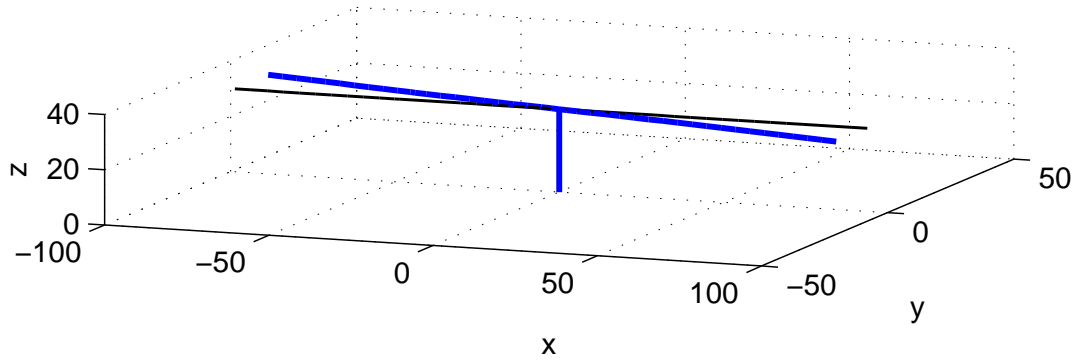


Figure 4.1: Response of mode 1 (for illustrative purpose multiplied by 30)

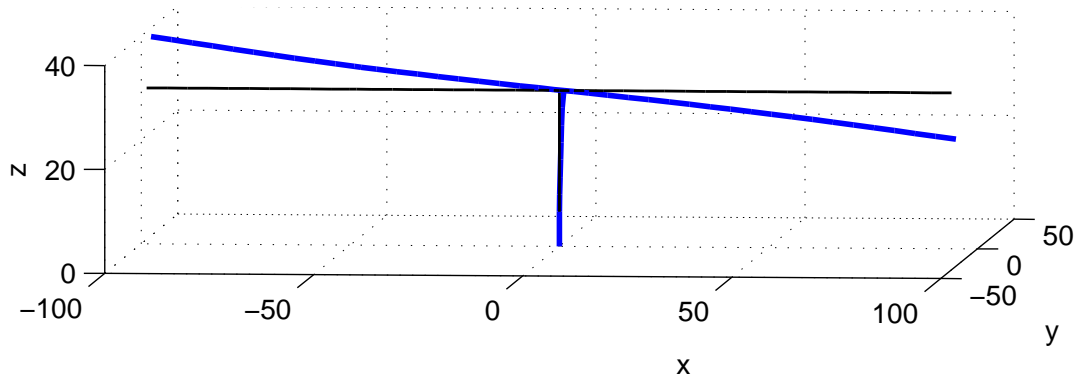


Figure 4.2: Response of mode 2 (for illustrative purpose multiplied by 30)

Possible sources of errors and sensitivity analysis of some of the parameters that were used in the calculations were researched. The structural damping is often an important element of uncertainty, however investigation showed that it had small influence on the calculated response. The buffeting aerodynamic damping was on the other hand relatively high, indicating that the assumption of negligible motion induced effects might introduce inaccuracy.

It was discovered that the choice of the constant elevation height of the girder had minor effect on the results.

It is uncertainty around the validity of the vortex shedding parameters as no experiments were performed towards finding values for this particular bridge and geographical position. Especially the nondimensional root mean square lift coefficient, $\hat{\sigma}_{q_z}$ was found to influence the calculated response significantly and could be a possible source of error.

It was also discovered that galloping might be an issue as the lift derivatives could contain negative values and reduce the total damping.

5 Suggestions for Further Research

An important issue when designing balanced cantilevered bridges is to avoid galloping. The derivative of the lift coefficient is a source of uncertainty towards galloping, and could thus be the object of further research.

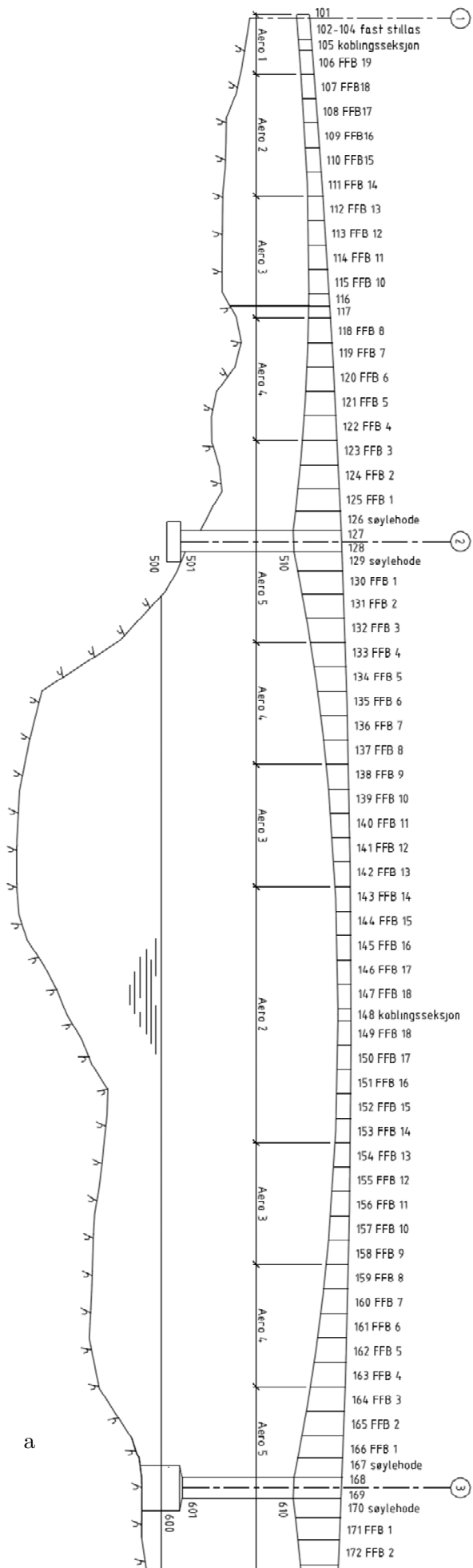
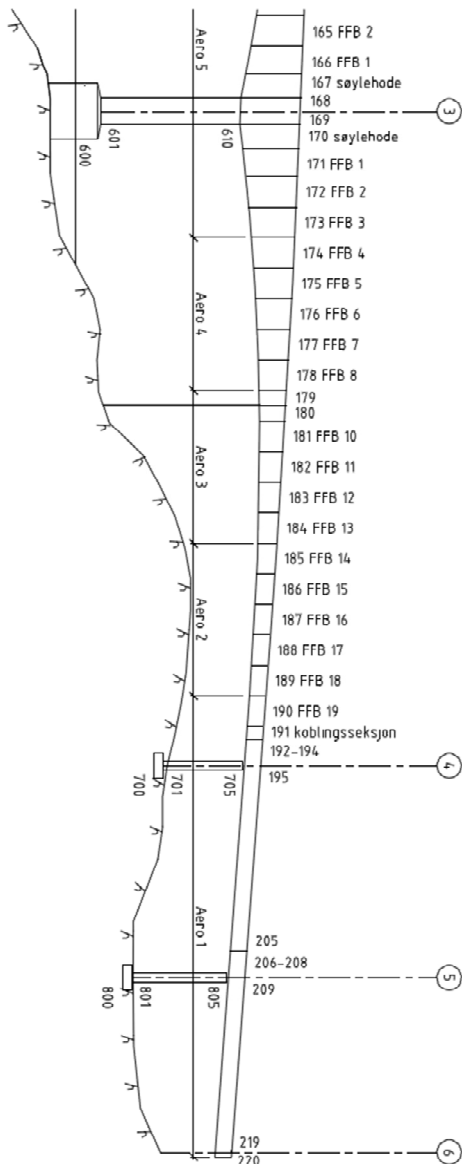
It is reason to believe that the vortex shedding induced response involves inaccuracies due to the many simplifications and assumptions that have been made. A natural follow-up to this report would be to perform vortex shedding tests on a model of the bridge with the objective to verify the properties and also compare the theoretical response to the measured response. Investigations towards developing the vortex shedding theory so it is applicable to structures with varying cross sectional dimensions could also be performed.

If the object is to perform a dynamic design control of the bridge there must be performed many more analyses both of other construction stages and of other dynamic loads, such as traffic loads, waves on the pillars and earthquakes.

References

- [1] E. N. Strømmen. *Theory of Bridge Aerodynamics*. Springer-Verlag Berlin Heidelberg, 2nd edition, 2010.
- [2] C. Dyrbye & S. O. Hansen. *Wind Loads on Structures. Appendix B*. John Wiley & Sons, 1st edition, 1997.
- [3] D. E. Newland. *An Introduction to Random Vibration and Spectral Analysis. Appendix 1*. Longman, 1st edition, 1975.
- [4] Statens Vegvesen. Fv-714 Dolmsundet, Bakgrunn. <http://www.vegvesen.no/Fylkesveg/fv714dolmsundet/Bakgrunn>, Mar 2013.
- [5] Wikipedia. Pierre Pflimlin Bridge. http://en.wikipedia.org/wiki/File: Pierre_Pflimlin_UC_AdjAndCrop.jpg, Mar 2013.
- [6] Statens Vegvesen. 16-1481 Dolmsundbrua, tegning nr. K316, Nov 2012.
- [7] E. Aune. Personal communication, Mar 7th 2013.
- [8] E. Aune. *Dolmsundbrua, Kapittel 2: Globalanalyse*. Statens Vegvesen, May 2012.
- [9] K. Harstveit. *Rapport nr. 34/99 klima, Dolmsundet bru, Vindforhold*. Det Norske Meteorologiske Institutt, Dec 1999.
- [10] K. Aas-Jakobsen Jr. & E. Strømmen. *Dynamic response of a box girder bridge during construction*. Journal of Wind Engineering into the 21st Century, Vol. 2, 1999.
- [11] J. H. Kaspersen E. Strømmen, E. Hjort-Hansen. *Dynamic loading effects of a rectangular box girder bridge*. Journal of Wind Engineering and Industrial Aerodynamics, Vol 89, 2001.
- [12] Comité Européen de Normalisation (CEN). *Eurocode 1: Actions on Structures, Part 1-4: General Actions, Wind Actions*, 2005.
- [13] E. N. Strømmen. Personal communication, Apr. 15th 2013.

A Definition of Elements



a

B Inputfile

%Element	%L_e[m]	%x[m]	%Height[m]	%Lump_mass [kN]	%Eig_vector1y	%Eig_vector2z	%Eig_vector2x	%Dragfact
106	2.4500	-98.7000	2.7500	48.6500	1.0000	1.0000	0.1247	5.9200
107	4.9000	-93.8000	2.7500	158.5000	0.9476	0.9411	0.1291	1.4000
108	4.9000	-88.9000	2.7680	97.4900	0.8952	0.8821	0.1335	1.4000
109	4.9000	-84.0000	2.8170	97.8600	0.8428	0.8234	0.1378	1.4000
110	4.9000	-79.1000	2.9000	99.1000	0.7904	0.7653	0.1419	1.4000
111	4.9000	-74.2000	3.0210	101.9000	0.7382	0.7080	0.1458	1.4000
112	4.9000	-69.3000	3.1820	105.7000	0.6861	0.6519	0.1494	1.7000
113	4.9000	-64.4000	3.3840	109.9000	0.6341	0.5972	0.1527	1.7000
114	4.9000	-59.5000	3.6300	114.3000	0.5825	0.5440	0.1557	1.7000
115	4.9000	-54.6000	3.9190	120.2000	0.5311	0.4924	0.1585	1.7000
116	3.6750	-50.1000	4.2540	85.3400	0.4801	0.4424	0.1610	1.7000
117	2.4500	-48.5000	4.4450	133.0000	0.4626	0.4254	0.1619	1.7000
118	3.6750	-44.8000	4.6350	120.7000	0.4296	0.3939	0.1634	2.0000
119	4.9000	-39.9000	5.0640	151.4000	0.3796	0.3467	0.1655	2.0000
120	4.9000	-35.0000	5.5410	158.2000	0.3301	0.3008	0.1675	2.0000
121	4.9000	-30.1000	6.0670	165.5000	0.2813	0.2560	0.1693	2.0000
122	4.9000	-25.2000	6.6430	173.3000	0.2332	0.2123	0.1710	2.0000
123	4.9000	-20.3000	7.2700	181.6000	0.1858	0.1695	0.1726	2.1800
124	4.9000	-15.4000	7.9480	192.7000	0.1393	0.1275	0.1740	2.1800
125	4.7000	-10.5000	8.6780	197.9000	0.0936	0.0863	0.1753	2.1800
126	4.0500	-6.0000	9.3940	185.3000	0.0524	0.0490	0.1764	2.1800
127	3.0000	-2.4000	10.0000	140.1000	0.0180	0.0177	0.1773	2.1800
128	2.4000	0.0000	10.0000	233.7000	0.0013	0.0000	0.1778	2.1800
129	3.0000	2.4000	10.0000	140.8000	-0.0207	-0.0176	0.1787	2.1800
130	4.0500	6.0000	9.3940	186.6000	-0.0550	-0.0489	0.1802	2.1800
131	4.7000	10.5000	8.6780	199.2000	-0.0960	-0.0860	0.1819	2.1800
132	4.9000	15.4000	7.9480	193.8000	-0.1414	-0.1270	0.1838	2.1800
133	4.9000	20.3000	7.2700	182.5000	-0.1875	-0.1686	0.1856	2.0000
134	4.9000	25.2000	6.6430	174.1000	-0.2342	-0.2109	0.1873	2.0000
135	4.9000	30.1000	6.0670	166.2000	-0.2815	-0.2539	0.1890	2.0000
136	4.9000	35.0000	5.5410	158.7000	-0.3294	-0.2978	0.1906	2.0000
137	4.9000	39.9000	5.0640	151.8000	-0.3778	-0.3426	0.1921	2.0000
138	4.9000	44.8000	4.6350	142.6000	-0.4267	-0.3884	0.1936	1.7000
139	4.9000	49.7000	4.2540	130.4000	-0.4759	-0.4353	0.1949	1.7000
140	4.9000	54.6000	3.9190	120.3000	-0.5255	-0.4833	0.1962	1.7000
141	4.9000	59.5000	3.6300	114.4000	-0.5754	-0.5325	0.1974	1.7000
142	4.9000	64.4000	3.3840	109.9000	-0.6255	-0.5829	0.1984	1.7000
143	4.9000	69.3000	3.1820	105.7000	-0.6757	-0.6343	0.1992	1.4000
144	4.9000	74.2000	3.0210	101.8000	-0.7261	-0.6866	0.1999	1.4000
145	4.9000	79.1000	2.9000	98.9300	-0.7766	-0.7396	0.2005	1.4000
146	4.9000	84.0000	2.8170	97.6200	-0.8271	-0.7931	0.2009	1.4000
147	4.9000	88.9000	2.7680	158.4000	-0.8776	-0.8468	0.2011	1.4000
148	2.4500	93.8000	2.7500	48.5500	-0.9282	-0.9004	0.2012	5.9200

C MATLAB Scripts

Input Scripts

```
% CALCULATES DISTRIBUTED MODAL MASS AND INTEGRATION OF EIGENMODES SQUARED

clear all
close all

% Length of elements:
L_el = dlmread('Inputfile.txt','','B2..B44');

% Number of elements:
n = length(L_el);

% Lumped mass:
m = dlmread('Inputfile.txt','','E2..E44');

% Eigenvectors:
Phi1 = dlmread('Inputfile.txt','','F2..F44');
Phi2 = dlmread('Inputfile.txt','','G2..G44');
Phi2x = dlmread('Inputfile.txt','','H2..H44');

% Defining variables:
Mmod1 = 0;
Mmod2 = 0;
IntPhi1 = 0;
IntPhi2 = 0;
IntPhi2_Lexp = 0;

% Integration over L:
for i = 1:n
    Mmod1 = Mmod1 + Phi1(i)^2*m(i)*L_el(i);
    IntPhi1 = IntPhi1 + Phi1(i)^2*L_el(i);

    Mmod2 = Mmod2 + (Phi2x(i)^2 + Phi2(i)^2) * m(i) * L_el(i);
    IntPhi2 = IntPhi2 + (Phi2x(i)^2 + Phi2(i)^2) * L_el(i);
end

% Integration over Lexp (for vortex calculations only):
for i = [1:13 33:43]
    IntPhi2_Lexp = IntPhi2_Lexp + (Phi2x(i)^2 + Phi2(i)^2) * L_el(i);
end

% Scaling to kg from kN (gravity Trondheim):
s = 1000/9.82;

% Modally equivalent evenly distributed mass:
m1 = (Mmod1/IntPhi1)*s;
m2 = (Mmod2/IntPhi2)*s;
```

```
% INPUT DATA

% Geometry:
B = 11.1;
L_el = dlmread('Inputfile.txt','','B2..B44');
x_vect = dlmread('Inputfile.txt','','C2..C44');
D = dlmread('Inputfile.txt','','D2..D44');
D_Vortex = 3.4;
```

```

% Load Coefficients:
Cd = dlmread('Inputfile.txt','','I2..I44');
Cl = 0.5;
Cdl = zeros(1,length(L_el));

% Wind Data (30 masl):
rho = 1.25;
% Buffeting:
I_n = [0.14 0.07]; % I_u and I_w
xL_n = [139.04 11.59]; % xFL_u and xFL_w
A_n = [1.08 1.50]; % A_u and A_w
c_nx = [9 6]; % c_ux and c_wx
V = 38.4;
% Vortex Shedding:
St = 0.11;
sigma_qz = 1;
b_z = 0.15;
a_z = 0.4;
lambda_z = 2;
K_az = 0.2;

% Eigenfrequencies:
omega_e = [1.401 1.687]; % omega_1 and omega_2
n_mod = length(omega_e);

% Damping:
zeta_e = 0.008; % for both modes

% Modal Mass:
m_e = [11528.01 11762.48]; % m_1 and m_2

% Eigenvectors:
Phi = [dlmread('Inputfile.txt','','F2..F44'); % mode 1: y-direction
       dlmread('Inputfile.txt','','G2..G44')]; % mode 2: z-direction

% Integral of eigenvectors squared:
IntPhi_e = [57.69 58.47]; % Int(Phi(1)^2)dx and Int(Phi(2)^2)dx over L
IntPhi_Lexp = 52.11; % Int(Phi(2)^2)dx over L_exp

```

Buffeting Scripts

```
function [S_n_red] = KaimalSpectralDensity(omega,A_n,xL_n,V)
    % Returns reduced Kaimal auto spectral density  $S_n/\sigma_n^2$  of the wind in
    % the direction of  $n = u$  ( $i=1$ ) and  $n = w$  ( $i=2$ )

    S_n_red = zeros(2,length(omega));

    for i = 1:2
        S_n_red(i,:) = (A_n(i)*xL_n(i))./(V*(1+1.5*A_n(i).*omega*(xL_n(i)/V))
            .^(5/3));
    end
```

```
function [Co_nn] = Co_spectrum(omega,Dx,c_nx,V)
    % Returns normalized co-spectrum of the turbulent wind in the direction of  $n =$ 
    %  $u$  ( $i=1$ ) and  $n = w$  ( $i=2$ )

    Co_nn = zeros(2,length(omega));

    for i = 1:2
        Co_nn(i,:) = exp(-c_nx(i) * (omega * Dx)/(2 * pi * V));
    end
```

```
function [zeta_ae] = AerodynamicDampingCoefficient(rho,V,B,D,Cd,Cdl,Phi,omega_e,
    m_e,L_el,dir,IntPhi_e)
    % Returns the buffeting aerodynamic damping coefficient

    Int = 0;
    n = length(L_el);

    if dir == 1 % Mode in y-direction
        for i = 1:n
            Int = Int + Phi(i)^2*D(i)*Cd(i)*L_el(i);
        end
    elseif dir == 2 % Mode in z-direction
        for i = 1:n
            Int = Int + Phi(i)^2*(B*Cdl(i)+D(i)*Cd(i))*L_el(i);
        end
    else
        disp('error')
    end

    zeta_ae = -(rho*V)/(2*omega_e*m_e) * Int/IntPhi_e;
```

```
function [abs_H] = FrequencyResponse(omega,rho,zeta_e,V,B,D,Cd,Cdl,L_el,dir,Phi,
    omega_e,m_e,IntPhi_e)
    % Returns the frequency response for mode  $\Phi_i$ 
    %  $dir = 1$  --> y-direction
    %  $dir = 2$  --> z-direction

    zeta_ae = AerodynamicDampingCoefficient(rho,V,B,D,Cd,Cdl,Phi,omega_e,m_e,L_el,
        dir,IntPhi_e);
    abs_H = abs(1 - (omega./omega_e).^2 + 2*i*(zeta_e-zeta_ae)*((omega./omega_e))
        ).^(-1);
```

```
function [Varnew] = Prolong(Var,div)
    % Prolongs Var into a longer function Varnew by interpolation, div = number of
    % divisions
```

```

n = length(Var);
Varnew = zeros(0,(n-1)*div+1);

Varnew(1) = Var(1);

for i = 0:n-2
    delta = (Var(i+2)-Var(i+1))/div;
    for j = 1:div
        Varnew(div*i+j+1) = Varnew(div*i+j) + delta;
    end
end

```

```

function [Varnew] = Expand(Var,div)
    % Expands Var into a new function Varnew, each value in Var is divided into
    % div values

n = length(Var);
Varnew = zeros(0,(n-1)*div+1);

Varnew(2:div) = (Var(1)+Var(2)*0.5)/div;
Varnew(1) = 0.5*Varnew(2);

for i = 1:n-3
    delta = (Var(i+1)+Var(i+2))/(2*div);
    Varnew(div*i+1:div*i+div) = delta;
    Varnew(div*i+div) = (delta + (Var(i+2)+Var(i+3))/(2*div))/2;
end

Varnew((n-2)*div+1:(n-1)*div) = (Var(n-1)*0.5+Var(n))/div;
Varnew((n-1)*div+1) = 0.5*Varnew((n-1)*div);
Varnew(div*(n-3)+div) = (delta + (Var(i+2)+2*Var(i+3))/(2*div))/2;

```

```

function [Jnorm] = JointAcceptance(omega,div,V,B,D,Cd,Cd1,L_el,c_nx,A_n,xL_n,
I_n,dir,Phi,IntPhi_e)
    % Returns the normalized joint acceptance function of mode Phi

    % Defining variables:
    Nomega = length(omega);
    J = zeros(1,Nomega);
    xi = 0;

    % The reduced Kaimal spectral density:
    S_n_red = KaimalSpectralDensity(omega,A_n,xL_n,V);

    % Linear prolongation/expandation of input variables:
    D = Prolong(D,div);
    Cd = Prolong(Cd,div);
    Cd1 = Prolong(Cd1,div);
    Phi = Prolong(Phi,div);
    L_el = Expand(L_el,div);

n = length(L_el);

    % Integration:
for i = 1:n
    Di = D(i);
    Cdi = Cd(i);
    Cdli = Cd1(i);
    L_eli = L_el(i);
    xi = xi + L_eli;
    Phii = Phi(i);

```

```

xj = 0;
for j = 1:n
    Dj = D(j);
    Cdj = Cd(j);
    Cdlj = Cdl(j);
    L_elj = L_el(j);
    xj = xj + L_elj;
    Phi_j = Phi(j);
    Dx = abs(xi-xj);
    Coij = Co_spectrum(omega,Dx,c_nx,V);
    if dir == 1 % mode in y-direction
        J = J + Phii * Phi_j .* ( ((2*I_n(1))/B)^2*Di*Cdi*Dj*Cdj) .* Coij
            (1,:) .* S_n_red(1,:) + (Cl*I_n(2))^2 .* Coij(2,:) .* S_n_red
            (2,:) * L_eli * L_elj;
    elseif dir == 2 % mode in z-direction
        J = J + Phii * Phi_j .* ( (2*Cl*I_n(1))^2 .* Coij(1,:) .* S_n_red
            (1,:) + ((I_n(2)^2*(Cdl+(Di*Cdi)/B)*(Cdlj+(Dj*Cdj)/B)) .*
            Coij(2,:) .* S_n_red(2,:)) * L_eli * L_elj;
    else
        disp('error')
    end
end
end

% Normalizing the joint acceptance function:
Jnorm = J/(IntPhi_e)^2;

```

```

function sigma_r = StandardDeviation(omega,div,rho,zeta_e,V,B,D,Cd,Cl,Cdl,L_el,
c_nx,A_n,xL_n,I_n,dir,Phi,omega_e,m_e,IntPhi_e)
% Calculates standard deviation of response along x-axis for mode Phi

Nomega = length(omega);
domega = (omega(Nomega)-omega(1))/(Nomega-1);
Int = 0;

% Frequency response function:
abs_H = FrequencyResponse(omega,rho,zeta_e,V,B,D,Cd,Cdl,L_el,dir,Phi,omega_e,
m_e,IntPhi_e);

% Normalized joint acceptance function:
Jnorm = JointAcceptance(omega,div,V,B,D,Cd,Cl,Cdl,L_el,c_nx,A_n,xL_n,I_n,dir,
Phi,IntPhi_e);

% Integration:
for i = 1:Nomega
    Int = Int + abs_H(i)^2*Jnorm(i);
end

% Standard deviation of the response:
sigma_r = abs(Phi) * ((rho*V^2*B)/(2*m_e*omega_e^2) * sqrt(Int*domega));

```

```

% PLOT STANDARD DEVIATION OF BUFFETING RESPONSE

```

```

clear all
close all

```

```

Input

```

```

% Choose integration accuracy:
omega = linspace(0,20,2000);
div = 4;

```

```

n = length(L_el);

sigma_r = zeros(n_mod,n);

for i = 1:n_mod
    sigma_r(i,:) = StandardDeviation(omega,div,rho,zeta_e,V,B,D,Cd,Cl,Cdl,L_el,
        c_nx,A_n,xL_n,I_n,i,Phi(i,:),omega_e(i),m_e(i),IntPhi_e(i));
    plot(x_vect,sigma_r(i,:), 'LineWidth',2)
    hold all
end

grid
xlabel('x [m]')
ylabel('\sigma_{r}(x) [m]')
legend('\sigma_{r_{y}}(x)', '\sigma_{r_{z}}(x)')

```

```

function S_r_dphi = ResponseSpectrum(omega,div,rho,zeta_e,V,B,D,Cd,Cl,Cdl,L_el,
    c_nx,A_n,xL_n,I_n,dir,Phi,omega_e,m_e,IntPhi_e)
    % Calculates response spectrum divided on Phi(x_r)

    % Frequency response function:
    abs_H = FrequencyResponse(omega,rho,zeta_e,V,B,D,Cd,Cdl,L_el,dir,Phi,omega_e,
        m_e,IntPhi_e);

    % Normalized joint acceptance function:
    Jnorm = JointAcceptance(omega,div,V,B,D,Cd,Cl,Cdl,L_el,c_nx,A_n,xL_n,I_n,dir,
        Phi,IntPhi_e);

    % Response spectrum:
    S_r_dphi = ((rho*V^2*B)/(2*m_e*omega_e^2))^2 * abs_H.^2.*Jnorm;

```

% TIME DOMAIN SIMULATIONS OF BUFFETING RESPONSE

```

clear all
close all

Input

% Fill in for sigma_r:
sigma_r = [0.139 0.076];

% Choose integration accuracy:
omega = linspace(0,20,2000);
div = 4;

N_omega = length(omega);
domega = (omega(N_omega)-omega(1))/N_omega;

% Simulate over 10 minutes' periodes:
t = linspace(0,600,600);
n_t = length(t);

% Define variables:
S_r_dphi = zeros(n_mod,N_omega);
S_r = zeros(n_mod,N_omega);
r = zeros(n_mod,n_t);

% Response at the tip of the cantilever:
for i = 1:n_mod
    Int=0;

```



```

        S_r_dphi(i,:) = ResponseSpectrum(omega,div,rho,zeta_e,V,B,D,Cd,C1,Cd1,L_el,
            c_nx,A_n,xL_n,I_n,i,Phi(i,:),omega_e(i),m_e(i),IntPhi_e(i));
        S_r(i,:) = S_r_dphi(i,:)*Phi(i,1)^2;
        % Peak factor:
        maxv = max(abs(r(i,:)));
        kp = maxv/sigma_r(i)
    end

    % Plot the response of time:
    subplot(2,1,1)
    plot(t,r(1,:))
    grid
    xlabel('T [s]')
    ylabel('r_y [m]')

    hold all

    subplot(2,1,2)
    plot(t,r(2,:))
    grid
    xlabel('T [s]')
    ylabel('r_z [m]')

```

```

% 3D PLOT OF RESPONSE MODE 1

```

```

clear all
close all

Input
n = length(L_el);
zoom = 30;
rmax = 0.44;
hold all

% Pillar initially:
xpillar0 = zeros(1,10);
ypillar0 = zeros(1,10);
zpillar0 = linspace(0,30,10);
plot3(xpillar0,ypillar0,zpillar0,'-b','Linewidth',2)

% Girder initially:
xgirder0 = x_vect;
ygirder0 = zeros(1,n);
zgirder0 = ones(1,n)*30;
plot3(xgirder0,ygirder0,zgirder0,'-k','Linewidth',1)

% Girder new:
xgirder = x_vect;
ygirder = zoom*rmax*Phi(1,:);
zgirder = zgirder0;
plot3(xgirder,ygirder,zgirder,'-b','Linewidth',2)

xlabel('x')
ylabel('y')
zlabel('z')
grid on
axis([-100 100 -50 50 0 40])

```

Vortex Shedding Scripts

```
function [zeta_ae] = AerodynamicDampingCoefficientV(B,D,rho,a_z,K_az,m_e,sigma_r,
    IntPhi_e,IntPhi_Lexp)

zeta_ae = ((rho*B^2*K_az)/(4*m_e)).*(1-(sigma_r./(a_z*D)).^2) *(IntPhi_e/
    IntPhi_Lexp);
```

```
function [Co_qz] = Co_spectrumV(D,lambda,Dx)
    % Calculates the normalized co-spectrum of vortex shedding in
    % z-direction
Co_qz = cos((2*Dx)./(3*lambda*D)) .* exp(-((Dx)./(3*lambda*D)).^2);
```

```
function S_Q = LoadSpectrumV(omega,rho,B,D,St,sigma_qz,b_z,lambda_z,IntPhi_Lexp,V)

omega_s = (2*pi*St*V)/D;
S_Q = 2*lambda_z*D * (((0.5*rho*V^2*B*sigma_qz)^2)/(sqrt(pi)*omega_s*b_z)) * exp
    (-((1-omega./omega_s)./b_z).^2) .* IntPhi_Lexp;
```

```
function sigma_r = StandardDeviationV(rho,B,D,St,sigma_qz,a_z,b_z,lambda_z,K_az,
    zeta_e,omega_e,m_e,Phi,IntPhi_e,IntPhi_Lexp,V)

% Resonant velocity:
V_R = (D*omega_e)/(2*pi*St);

% Temporary variables:
zeta_hat = ((4*m_e*zeta_e)/(rho*B^2*K_az))*(IntPhi_e/IntPhi_Lexp);
beta_hat = Phi/(2^(5/2)*pi^(7/4)) * ((rho*D^3*lambda_z)/(m_e*b_z*K_az*IntPhi_e))
    ^((1/2) * (sigma_qz/(St^2*a_z)) * (V/V_R)^(3/2) * exp(-(1/2)*((1-(V_R/V))/b_z)
    ^2));

% Solves the fourth order polynomial:
sigma_hat = ((1-zeta_hat)/2 + (((1-zeta_hat)/2)^2 + beta_hat^2)^(1/2))^(1/2);

% Standard deviation of displacement:
sigma_r = sigma_hat*a_z*D;
```

```
% PLOT STANDARD DEVIATION OF VORTEX SHEDDING RESPONSE

clear all
close all

Input

omega_e = omega_e(2);
m_e = m_e(2);
IntPhi_e = IntPhi_e(2);
n = length(L_el);

% Plots the standard deviation for different velocities:
V = linspace(0,20,10000);
n_V = length(V);
Phii = Phi(2,1); % Mode 2 evaluated in x = -98.7 m
sigma_r = zeros(1,n_V);

for i = 1:n_V
    Vi = V(i);
    sigma_r(i) = StandardDeviationV(rho,B,D_Vortex,St,sigma_qz,a_z,b_z,lambda_z,
        K_az,zeta_e,omega_e,m_e,Phii,IntPhi_e,IntPhi_Lexp,Vi);
```

```

end

subplot(2,1,1)
plot(V,sigma_r,'Linewidth',2)
ylabel('\sigma_{r_{z}}(x = -98.7) [m]')
xlabel('V [m/s]')
grid
axis([0 20 0 0.15])

% Plots the standard deviation along the girder at resonant wind velocity:
V = (D_Vortex*omega_e)/(2*pi*St);
sigma_r = zeros(1,n);

for i = 1:n
    Phii = Phi(2,i);
    sigma_r(i) = StandardDeviationV(rho,B,D_Vortex,St,sigma_qz,a_z,b_z,lambda_z,
        K_az,zeta_e,omega_e,m_e,Phii,IntPhi_e,IntPhi_Lexp,V);
end

subplot(2,1,2)
plot(x_vect,sigma_r,'Linewidth',2)
ylabel('\sigma_{r_{z}}(x) [m]')
xlabel('x [m]')
grid
axis([-100 100 0 0.15])

```

```

% TIME DOMAIN SIMULATION OF VORTEX SHEDDING RESPONSE

clear all
close all

Input

omega = linspace(0,20,2000);
N_omega = length(omega);
domega = (omega(N_omega)-omega(1))/N_omega;

t = linspace(0,600,600);
n_t = length(t);

% Define the mode for which vortex shedding may be a problem:
Phii = Phi(2,1); % Largest displacement --> left tip of the cantilever
omega_e = omega_e(2);
m_e = m_e(2);
IntPhi_e = IntPhi_e(2);

% Fill in for sigma_r:
sigma_r = 0.130;

% Resonant velocity:
V = (D_Vortex*omega_e)/(2*pi*St);

% Aerodynamic damping coefficient:
zeta_ae = AerodynamicDampingCoefficientV(B,D_Vortex,rho,a_z,K_az,m_e,sigma_r,
    IntPhi_e,IntPhi_Lexp);

% Frequency response function:
abs_H = abs(1 - (omega./omega_e).^2 + 2*1i*(zeta_e-zeta_ae)*((omega./omega_e)))
    .^(-1);

```

```

% Load spectrum:
S_Q = LoadSpectrumV(omega,rho,B,D_Vortex,St,sigma_qz,b_z,lambda_z,IntPhi_Lexp,V);

% Response spectrum:
S_r = ((Phi_i^2*abs_H.^2)./((omega_e^2*m_e*IntPhi_e).^2)).*S_Q;

r = zeros(1,n_t);
int=0;

% Response at the tip of the cantilever:
for i = 1:N_omega
    r = r + sqrt(2*S_r(i)*domega) .* cos(omega(i)*t - rand(1)*2*pi);
    int = int + S_r(i);
end

% Max value:
maxz = max(abs(r));
kpz = maxz/sigma_r

% Plot the response of time:
plot(t,r)
grid
xlabel('T [s]')
ylabel('r_z [m]')

```

% 3D PLOT OF RESPONSE MODE 2

```

clear all
close all

Input
n = length(L_el);
zoom = 30;
rmax = 0.33;
hold all

% Pillar initially:
xpillar0 = zeros(1,10);
ypillar0 = zeros(1,10);
zpillar0 = linspace(0,30,10);
plot3(xpillar0,ypillar0,zpillar0,'-k','Linewidth',1)

% Girder initially:
xgirder0 = x_vect;
ygirder0 = zeros(1,n);
zgirder0 = ones(1,n)*30;
plot3(xgirder0,ygirder0,zgirder0,'-k','Linewidth',1)

% Pillar new:
xpillar = zoom*rmax
*[0,0.00043,0.00349,0.00929,0.01761,0.02823,0.04092,0.05546,0.07163,0.10794];
ypillar = zeros(1,10);
zpillar = linspace(0,30,10);
plot3(xpillar,ypillar,zpillar,'-b','Linewidth',2)

% Girder new:
xgirder = x_vect + xpillar(10);
ygirder = zeros(1,n);
zgirder = 30 + zoom*rmax*Phi(2,:);
plot3(xgirder,ygirder,zgirder,'-b','Linewidth',2)

```

```
xlabel('x')
ylabel('y')
zlabel('z')
grid on
axis([-100 100 -50 50 0 40])
```